Modified Stability Equations for Pre-Twisted Columns

A THESIS

SUBMITTED TO THE FACULTY OF THE

UNIVERSITY OF MINNESOTA BY

Martin Ramaswamy

IN PARTIAL FULFILLMENT OF THE REQUIREMENTS

FOR THE DEGREE OF

MASTER OF SCIENCE

Advisor: Professor Henryk Stolarski

January 2023

Abstract.

It is shown that the theory of pre-twisted bars used in all existing publications on the subject violates the traction boundary conditions on the side surfaces of those bars. A simple modification is proposed to satisfy those conditions without changing anything in the basic kinematic structure of the theories currently in use. Stability of pre-twisted bars is used in this work to present and illustrate the new, modified theory. There are two specific outcomes of that new formulation, one is emergence of torque as an additional internal force generated by the axial load, and the other is the reduction of the bending stiffness in pre-twisted bars. Of the two, the former turns out to be rather negligible, but the latter is quite significant and, comparing to the current theory, changes the buckling load of pre-twisted bars rather significantly. This is illustrated by a number of numerical examples.

TABLE OF CONTENTS

List of Figures:

1. Introduction

Pre-twisted bar-like structures can be found in various environments. The oldest examples of such structures are found in nature which, in an effort to optimize its creations, produced many of them as a result of natural evolution. The DNA helix (Lotz et al., 1982; Ji et al., 2012) is arguably the best known of them. Other examples include some bacteria and tissues (Wang, 1997; Schulgasser and Witztum, 2004a, 2004b; Wang, 2013).

There are also many examples of pre-twisted structures in engineering. Columns in many ancient civil and religious structures appear pre-twisted, but mostly for decorative reason. In modern applications such as jet engine blades, helicopter rotor blades, wind turbine blades etc., the twisted geometry plays an essential role in the function of the structure (Sinha, 2007; Le, et al., 2020).

All structures, those existing in nature and those in the man-made environment, are under the action of various forces, and mechanical analysis has to be performed if the response to those forces needs to be determined. Mechanical analysis of various engineering problems has been a tool of engineers for centuries and there are volumes of publications on the subject. However, in the last several decades mechanical analysis has been found useful in advancing understanding of various biological phenomena. Special models, often coupling mechanical and other (chemical, biological etc.) aspects of the problem have been developed, and the literature covering those applications is rapidly growing (e.g. Zhao et al., 2014; Gilmanov et al., 2018; Gangwar et al., 2021; Hamilton et al., 2022)

Stability of biological and engineering structures is one of several important issues requiring a somewhat specialized approach rooted in nonlinear analysis. In its most basic form, the problem has its basis in Lyapunov stability which states that a system is stable if a small input perturbation will generate a small output result. In the problem applying an axial load to the column will result in two possible deformation scenarios to produce material strain to counter the work done by the axial force, one option is for

the column to shrink axially, and another option is to bend into a deformed configuration. If the load is applied directly to the undeformed configuration there is a point at which a small deflection perturbation in the system will generate a large amount of deflection, hence the system is unstable. In particular, stability analysis of pre-twisted bars involves an additional level of complexity related to its initial geometry. This type of phenomena has been the subject of investigations a long time ago (Ziegler, 1951) and continues to be of interest till now (Anliker and Troesch, 1963; Carnegie, 1964; Zhao et al., 2014). The problem was addressed mostly analytically (Frisch-Fay, 1973; Steinman, 1989; Tabarrok et al., 1990), including numerical analyses (Abid, 2008; Zhao et al., 2014), but there were also some involving experimental investigations (Megahed, 2015). Majority of the analytical investigations are based on quite common (Euler-Bernoulli) assumptions: that the cross sections remain orthogonal to the deforming axis of the bar throughout the process; that they remain flat during buckling; and that they do not deform within their planes. Those assumptions have been proven to be very adequate in analysis of slender structures, including bars whose stability is particularly important when they are slender. Thus, Euler-Bernoulli assumptions are also adopted in this work. Nonetheless, some of the publications on the subject, particularly those employing numerical solution methods, abandon the orthogonality assumption and allow for transverse shear deformation (Celep. 1984; Tabarrok et al., 1990; Zhu, 2011; Zhao et al., 2014), which is the basis of another well-known model used in structural analysis (Timoshenko model).

A more technical distinction between various approaches relates to the way deformation of pre-twisted bars is described, and either of them can be adopted regardless of what particular model is used. In some of them the transverse displacements of the bars, and their constitutive equations, were related to the local orthogonal coordinate system whose axes are aligned with the principal axes of the cross sections (Tabarrok et al., 1990) and, thus, vary along the length of the bar. In others they are related to a global, fixed and orthogonal coordinate system (Zhao et al.,

2014). Those two approaches are, of course, completely equivalent, as long as they are based on the same set of underlying assumptions.

Irrespectively of what coordinate systems have been used in the description of the problem the publications on pre-twisted bars can be divided into two groups: One using the Euler-Bernoulli model and the other using the Timoshenko model. Within each of those groups the difference between publications is essentially limited to what specific problems were solved, what method were used to solve them and what issues were discussed. All those contributions were important but, still, the theory used was essentially the same. In particular, in all theories used to analyze pre-twisted bars, the normal stress components were linearly distributed over the cross sections and related to the bar curvatures in exactly the same way as in the case of prismatic bars. As a result, for pre-twisted bars none of them satisfied the traction-free boundary conditions on their side faces, which is a drawback.

A modification of the theory that allows to correct the current problem with the traction-free boundary conditions is proposed in this work. It is shown that it can be achieved by a simple modification of the way the stresses are evaluated, and with total preservation of the basic kinematic structure of the theory. As a result, the normal stresses are not linearly distributed over the bar cross sections, which is a departure from what has been done till now. This constitutes the main conceptual contribution of this work. Quantitative analysis of the effects the proposed modifications entail is a natural second contribution, which demonstrates that the proposed changes are quite important.

The presentation of the arguments advanced in this work is organized as follows. In the next section, Section 2, the problem parametrization, referred to in various parts of this work, and the basic strain and stress state analysis is discussed to motivate the proposed modifications. This is followed by two sections presenting different formulations of the pre-twisted bar's stability problem. In Section 3 the formulation is based on the column equilibrium equations expressed in terms of the resultant forces

and resultant moments, and in Section 4 the energy formulation is presented starting with a bar as a three-dimensional body. In both cases the stability equations are obtained in the standard way - by superposing small variations on the pre-existing finite stress states. Section 5 is designed to present a discussion and critical evaluation of the proposed modifications. Numerical methods are presented in Section 6, and the results of this work are presented in section 7, whereas the final section, Section 8, contains some concluding comments.

2. On strain and stress states in pre-twisted bars.

2.1. Kinematics of pre-twisted bars.

As typically done, it is assumed here that the pre-twisted bar's volume is traced by a cross section of fixed geometry that rotates around its centroid as it moves along its straight axis. The shape of the cross section can be arbitrary, but the most common shape is rectangular; that shape is illustrated in Fig. 1 and is used in the subsequent numerical examples. The volume of the bar is parametrized by the curvilinear coordinates $\xi^1, \xi^2, \xi^3, (\xi^1 = x^1)$ such that the position vector described in the global, rectangular coordinate system x^1, x^2, x^3 has the form

$$\boldsymbol{R}(\xi^K) = \xi^1 \boldsymbol{e_1} + \left[\xi^2 \cos\left(\theta(\xi^1)\right) - \xi^3 sin\left(\theta(\xi^1)\right)\right]\boldsymbol{e_2} + \left[\xi^2 sin\left(\theta(\xi^1)\right) + \xi^3 \cos\left(\theta(\xi^1)\right)\right]\boldsymbol{e_3} \quad (1)$$

where vectors $\boldsymbol{e_K}$, $K = 1,2,3$, are unit and parallel to the global, orthogonal axes x^K, shown in Fig. 1. As is clear from the above equation, $-{}^{a}/_{2} \leq \xi^2 \leq {}^{a}/_{2}$ and $-{}^{b}/_{2} \leq \xi^3 \leq {}^{b}/_{2}$ parametrize the cross sections of the bar, and their range of variation is the same for all cross sections, whereas the angle $\theta(\xi^1)$, $0 \leq \xi^1 \leq L$, represents the angle of twist. Clearly, the dimension of the bar cross section is a x b and L is its

length. eq. (1) also reveals that the twist is positive if the vector representing that twist, defined with the right-hand rule, is aligned with the positive direction of x^1.

The parametric lines $\xi^2 = const$ *and* $\xi^3 = const$ (ξ^1*-lines,* that is*)* have helical form, as identified in the top part of Fig.1. The vectors of the natural basis associated with the above parametrization are

$$\boldsymbol{G}_K = \frac{\partial \boldsymbol{R}}{\partial \xi^K} = \boldsymbol{R}_{,K}\,, \quad K = 1,2,3 \tag{2}$$

While the vectors $\boldsymbol{G}_2$ and $\boldsymbol{G}_3$ are unit and orthogonal to each other (and they are located in the planes of the cross sections), they are not orthogonal to $\boldsymbol{G}_1$, which is tangent to the helical ξ^1*-line.* Vectors $\boldsymbol{G}_1$, tangnt to the helical ξ^1*-lines*, will be of particular importance in various parts of the subsequent development and they have the form

$$\boldsymbol{G_1} = \boldsymbol{e_1} + \alpha\{\left[-\xi^2 \sin\left(\theta(\xi^1)\right) - \xi^3 cos\left(\theta(\xi^1)\right)\right]\boldsymbol{e_2} + \left[\xi^2 cos\left(\theta(\xi^1)\right) - \xi^3 \sin\left(\theta(\xi^1)\right)\right]\boldsymbol{e_3}\} =$$

$$= \boldsymbol{e_1} + \alpha\{[-x^3]\boldsymbol{e_2} + [x^2]\boldsymbol{e_3}\} \tag{3a}$$

The length of those vectors is

$$|\boldsymbol{G}_1| = \sqrt{\boldsymbol{G}_1 \cdot \boldsymbol{G}_1} = \sqrt{G_{11}} = (1 + \alpha^2\rho^2)^{1/2} \tag{3b}$$

where $\alpha = \theta_{,1}$ is the rate of twist and $\rho = [(\xi^2)^2 + (\xi^3)^2]^{1/2}$ is the distance from the cross-section's centroid to the point specified by the coordinates (ξ^2, ξ^3), as shown in Fig. 1.

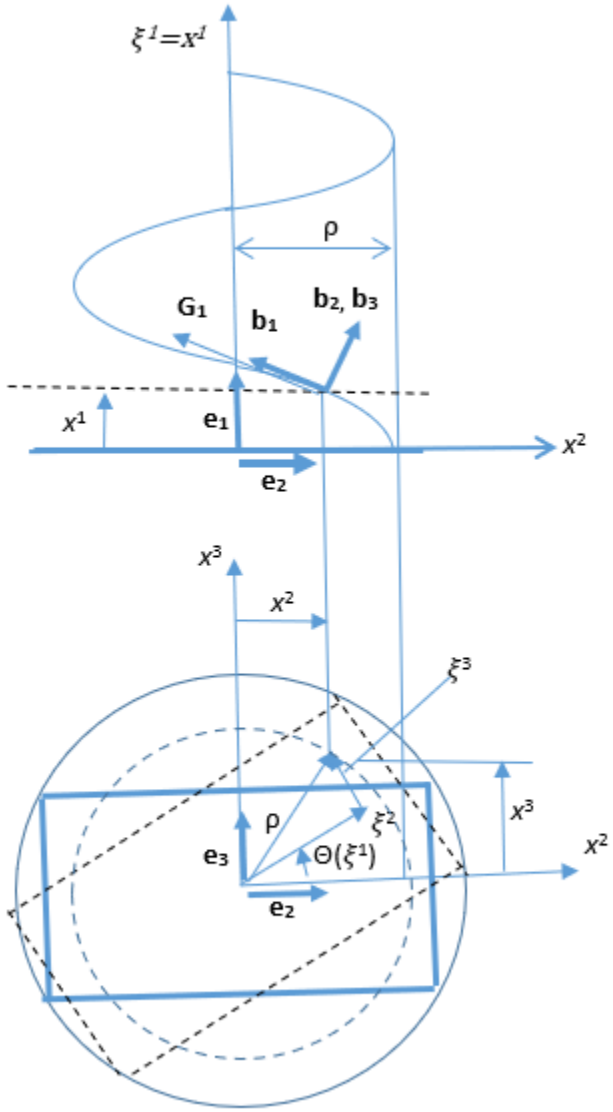

Fig.1. Parametrization and vector bases used in the formulation.

The modified theory of pre-twisted bars will be presented in this work in the context of bar's stability. In addition, the bars discussed here are slender, so the usual (Euler-Bernoulli) assumptions appropriate for bending of slender bars are made. Thus, in the process of deformation the cross sections are flat, they preserve their dimensions *a* x *b,* and they remain orthogonal to the deforming centroidal axis of the bar.

To make the main arguments advocated in this work more transparent, the attention is first directed to pure axial tension (or compression) of pre-twisted slender columns, which is the initial state stability of which is to be investigated. With the displacement at $x^1=0$ assumed to vanish, the displacement field associated with such a state, and obeying the kinematic assumptions made in the previous paragraph for slender bars, has the form

$$\boldsymbol{u}(x^K) = u_L \frac{x^1}{L}\, \boldsymbol{e}_1 \tag{4}$$

The definition of the strain field associated with such displacement field is unique in the small strain case and it is

$$\boldsymbol{\varepsilon} = \nabla_S \boldsymbol{u} = \frac{u_L}{L} \boldsymbol{e}_1 \otimes \boldsymbol{e}_1 = \varepsilon_{11} \boldsymbol{e}_1 \otimes \boldsymbol{e}_1 \tag{5a}$$

In the large deformation case several different strain measures are available, of which the following Cauchy-Green definition is probably the most popular, and will be used in this work in the sequel,

$$\boldsymbol{E} = \nabla_S \boldsymbol{u} + \frac{\mathbf{1}}{\mathbf{2}} \nabla^T \boldsymbol{u} \nabla \boldsymbol{u} = \left[\frac{u_L}{L} + \frac{1}{2} \left(\frac{u_L}{L} \right)^2 \right] \boldsymbol{e}_1 \otimes \boldsymbol{e}_1 = E_{11} \boldsymbol{e}_1 \otimes \boldsymbol{e}_1 \tag{5b}$$

In both of the above equations ∇ represents the gradient operator, the subscript S signifies its symmetric part, and the superscript T denotes transposition. The basis for the Cauchy-Green strain tensor is the effective mapping of the undeformed configuration to the deformed configuration. This can be compared to the similar strain measurements in 1-d and 2-d where the mapping in one dimension works by evaluating the ratio of the deflection to the total length of the member; this in effect gives enough

information to map between the deformed and undeformed configurations. Similarly, the strain tensor is a 3-d version that allows a linear and continuous mapping between configurations. This is accomplished by establishing a material point within the body and then relating the positional vector between the undeformed and deformed configuration.

As expected, in both cases the resulting strain states are one-dimensional, with the only strain component different from zero being the one representing stretching of the lines parallel to the axis of the bar. In the coordinate system x^K the small strain state of that kind is described by the following matrix

$$[\varepsilon] = \begin{bmatrix} \varepsilon_{11} & 0 & 0 \\ 0 & 0 & 0 \\ 0 & 0 & 0 \end{bmatrix} \tag{6}$$

The matrix for the large deformation problem has the same form but E_{11} is present instead of $\varepsilon_{11.}$

Under the assumptions specified earlier for slender bars the strain field within the volume of the column associated with bending is also described by eq. (6). However, the formulas specifying ε_{11} or E_{11} are different than those presented in either eq. (5a) od eq. (5b). As is well known, in the case of the small strain bending problems ε_{11} depends linearly on x^2 and x^3 (or ξ^2 and ξ^3), and its dependence on ξ^1 depends on bending in x^1-x^2 and x^1-x^3 plane. The formulas specifying that dependence will be provided in subsequent sections of this work.

2.2. On the stress state in the pre-twisted bars. Axial load case.

Based on known prior publications in the literature on the stability of pre-twisted bars, the stress matrix related to the global coordinates x^K also has the form specified for strains in eq. (6), but with σ^{11} replacing $\varepsilon_{11.}$ This is the consequence of the one-dimensional constitutive equation $\sigma^{11} = E\,\epsilon_{11}$, commonly used in analysis of pre-twisted columns, with E being the (Young) modulus of elasticity. Such constitutive

equation is applied both to pre-buckled deformations and to deformations associated with buckling itself, which necessarily includes small bending. In the case of bending, this constitutive equation leads to the well-known formulas specifying bending moments to be proportional to the cross-sectional moments (and products) of inertia.

For the existing formulations of the pre-twisted bar problems to be physically justified, the lines parallel to the axis of the beam, passing through every point of each cross section, must be capable of supporting the stress $\sigma^{11} = E\ \epsilon_{11}$ associated with that point. To see that it is unrealistic, consider one of the corner points of an arbitrary (e.g. rectangular) cross section. As the cross section moves along the bar's axis and rotates that point traces a helix with the largest radius ρ (cf. Fig 1). Clearly, a line parallel to the axis of the bar and passing through that corner point of the considered cross section is located entirely outside of the volume of the bar. In fact, it can only have a number of isolated points common with that volume (depending on the number of rotations), which are the points of the corner helixes with the same radius ρ. Although, from the kinematic viewpoint, that line may be considered to deform according to eq. (6), it is unphysical to assume that the above one-dimensional constitutive equation is applicable to it. That logic is directly adopted from the theory of prismatic (untwisted) bars, where it is valid.

Lines parallel to the bar's axis in the vicinity of the corners have a short segment in common with the volume of the bar, but the assumption that a short overlapping segment is enough to develop the full stress predicted by the one-dimensional constitutive equation used in prior publications is also questionable. Thus, it seems that in the existing formulations of the pre-twisted bars' stability, the contribution of the corner zones to the bending stiffness of the bars may be overestimated by using the one-dimensional constitutive equations discussed above. Importance of what happens at the corner zones has, of course, to do with their large distance from the centroids, and dependence of the bending stiffness on moments and products of inertia. Considering that bending stiffness of the bar has a critical effect on its stability, it

appears that reexamination of the problem is justified. The observation described above motivated the investigations presented in this work.

To examine the plausible state of stress in the vicinity of corners, a general, fully three-dimensional state of stresses at a corner is initially assumed. It can be represented by a full matrix related to any vector basis (or to the associated tensor basis), but the discussion presented here is easier if it is referred to the orthonormal vector basis $\boldsymbol{b}_K$, attached to some point of a corner helix (cf. Fig. 1) and defined as follows: *Vector* $\boldsymbol{b}_1$ is tangent to the helix, so

$$\boldsymbol{b}_1 = \frac{\boldsymbol{G}_1}{|\boldsymbol{G}_1|} \tag{7}$$

while the other two are any vectors orthogonal to it, and to each other. Of course, vectors $\boldsymbol{b}_K$ can be specified for the helix traced by any point of the cross section, not just corner helix, and then they vary with coordinates ζ^K; those vectors will be used subsequently. The initial stress matrix related to that basis is denoted by $[\overline{\overline{\boldsymbol{\sigma}}}]$ and its initial, general form is assumed to be

$$[\overline{\overline{\boldsymbol{\sigma}}}] = \begin{bmatrix} \bar{\bar{\sigma}}^{11} & \bar{\bar{\sigma}}^{12} & \bar{\bar{\sigma}}^{13} \\ \bar{\bar{\sigma}}^{21} & \bar{\bar{\sigma}}^{22} & \bar{\bar{\sigma}}^{23} \\ \bar{\bar{\sigma}}^{31} & \bar{\bar{\sigma}}^{32} & \bar{\bar{\sigma}}^{33} \end{bmatrix} \tag{8}$$

Then, the fact that side surfaces of the pre-twisted bar are load-free (or traction-free) is exploited to make eq. (8) more specific. To this end the normal vectors to the two side surfaces, intersection of which forms the corner helix, are denoted by $\boldsymbol{n}$ and $\boldsymbol{m}$, respectively. Since $\boldsymbol{b}_1$ is tangent to both surfaces, vectors $\boldsymbol{n}$ and $\boldsymbol{m}$ are orthogonal to $\boldsymbol{b}_1$ - they are then located in the plane defined by vectors $\boldsymbol{b}_2$ and $\boldsymbol{b}_3$. As a result, one has

$$\boldsymbol{n} = n^2\boldsymbol{b}_2 + n^3\boldsymbol{b}_3 \tag{9a}$$

$$\boldsymbol{m} = m^2\boldsymbol{b_2} + m^3\boldsymbol{b}_3 \tag{9b}$$

The traction-free conditions on the surfaces with those normal vectors are

$$\begin{bmatrix}0\\0\\0\end{bmatrix} = \begin{bmatrix}\bar{\bar{\sigma}}^{11} & \bar{\bar{\sigma}}^{12} & \bar{\bar{\sigma}}^{13}\\ \bar{\bar{\sigma}}^{21} & \bar{\bar{\sigma}}^{22} & \bar{\bar{\sigma}}^{23}\\ \bar{\bar{\sigma}}^{31} & \bar{\bar{\sigma}}^{32} & \bar{\bar{\sigma}}^{33}\end{bmatrix}\begin{bmatrix}0\\n^2\\n^3\end{bmatrix} = \begin{bmatrix}\bar{\bar{\sigma}}^{11} & \bar{\bar{\sigma}}^{12} & \bar{\bar{\sigma}}^{13}\\ \bar{\bar{\sigma}}^{21} & \bar{\bar{\sigma}}^{22} & \bar{\bar{\sigma}}^{23}\\ \bar{\bar{\sigma}}^{31} & \bar{\bar{\sigma}}^{32} & \bar{\bar{\sigma}}^{33}\end{bmatrix}\begin{bmatrix}0\\m^2\\m^3\end{bmatrix} \tag{10}$$

This requirement can only be fulfilled if

$$[\bar{\bar{\boldsymbol{\sigma}}}] = \begin{bmatrix}\bar{\bar{\sigma}}^{11} & 0 & 0\\ 0 & 0 & 0\\ 0 & 0 & 0\end{bmatrix} \tag{11}$$

The above result implies that while the state of stress at a corner of the cross section is still one-dimensional, that stress cannot be aligned with the direction of the column axis but is tangent to the corner helix. That conclusion is based on elementary continuum mechanics formulas and, of course, was anticipated.

The above conclusion is precisely valid only for the corner helix, but what happens at other points of the cross section cannot be argued equally rigorously and some assumptions have to be made. However, the goal for those assumptions should always be to fulfill as many as possible conditions that the stress distribution associated with the exact solution of the problem (whatever it is) satisfies. In that spirit, first, it is reasonable to assume that the exact stress distribution (including direction of tractions) over the cross section is continuous. Second, the exact distribution of stresses is associated with vanishing tractions over each entire side surface of the column, not just in the vicinity of corners. And third, for slender bars, it is reasonable to assume that the state of stress at every point within the volume of the bar is still one-dimensional, just as assumed in prismatic bars or in previous analyses of pre-twisted bars. One plausible assumption guaranteeing satisfaction of all those requirements is that at every point of the cross section the situation is similar to that at the corner points. *Under this assumption the state of stress at each point of the cross section is one-dimensional and, relative to the local basis* $\boldsymbol{b}_K$ *associated with the helix traced by that point, is defined by eq. (11).* That stress is tangent to the local helix passing through that point of the cross

section, and not parallel to the axis of the column. All subsequent developments are based on this assumption.

The assumption made in the previous paragraph implies that the non-vanishing stress component $\bar{\bar{\sigma}}^{11}$ of eq. (11) is acting on the plane perpendicular to the helix passing through a considered point of the cross section. To define the stress resultants needed to formulate some of the other relevant equations used later in this work the stresses acting on the plane of the cross section (or tractions) are needed. Given that the unit vector perpendicular to the column cross sections is $\boldsymbol{e}_1$, the stress vectors acting at a generic point of the cross section, $\boldsymbol{t}_1$, is

$$\boldsymbol{t}_1 = [\bar{\bar{\boldsymbol{\sigma}}}]\boldsymbol{e}_1 \tag{12}$$

However, considering that the stress matrix of eq. (10) is defined relative to the basis $\boldsymbol{b}_K$, in eq. (11) vector $\boldsymbol{e}_1$ should be represented by the components related to the same basis $\boldsymbol{b}_K$, and so will be the resulting vector $\boldsymbol{t}_1$. Consequently,

$$\boldsymbol{t}_1 = \bar{\sigma}^{11}(\boldsymbol{e}_1 \cdot \boldsymbol{b}_1)\boldsymbol{b}_1 \tag{13}$$

With the help of eqs. (3a), (3b) and (7), a more specific form of $\boldsymbol{t}_1$ can be found to be

$$\boldsymbol{t}_1 = \frac{\bar{\sigma}^{11}}{1+\alpha^2\rho^2}\boldsymbol{G}_1 \tag{14}$$

eq. (14) (as well as eq. (13)) shows that arguments advocated here lead to the conclusion that the stresses applied to each cross section of a twisted bar include both normal and shear components. It is so because vector $\boldsymbol{G}_1$ (or $\boldsymbol{b}_1$) is perpendicular to the plane of the cross section only at its centroid. And that direction of local stress should occur even for pure axial tension or compression.

The normal and shear components of the stresses acting on the plane of the cross section can be further specified considering eq. (3a)

$$\boldsymbol{t}_1 = \begin{bmatrix}\sigma^{11}\\ \sigma^{12}\\ \sigma^{13}\end{bmatrix} = \frac{\bar{\sigma}^{11}}{1+\alpha^2\rho^2}\begin{bmatrix}1\\ \alpha\left[-\xi^2\, sin\left(\theta(\xi^1)\right) - \xi^3 cos\left(\theta(\xi^1)\right)\right]\\ \alpha\left[\xi^2 cos\left(\theta(\xi^1)\right) - \xi^3\, sin\left(\theta(\xi^1)\right)\right]\end{bmatrix} \tag{15}$$

2.3. Constitutive equations for pre-twisted bars.

In linear elasticity, the one-dimensional state of stress at every point of the pre-twisted bar, which, as argued here, is aligned with the tangent to the local helixes, should be linearly related to the amount of local stretching those helixes experience. This is analogous to what is done in all existing publications, only they assume that the one-dimensional stress at every point is aligned with the axis of the column.

The strain that the helixes experience is $\bar{\epsilon}_{11}$ component of the strain given by the matrix of eq. (6), but expressed in relation to the basis $\boldsymbol{b}_K$, not relative to $\boldsymbol{e}_K$ as presented in eq. (6). Consequently, considering eqs. (3a), (3b) and (7),

$$\bar{\epsilon}_{11} = \boldsymbol{b}_1^T[\epsilon]\boldsymbol{b}_1 = \frac{\epsilon_{11}}{1+\alpha^2\rho^2} \tag{16}$$

and

$$\bar{\sigma}^{11} = E\bar{\epsilon}_{11} = \frac{E\epsilon_{11}}{1+\alpha^2\rho^2} \tag{17}$$

With that result the normal and shear stresses acting on the cross section and given in eq. (15) have the following final form

$$\begin{bmatrix}\sigma^{11}\\ \sigma^{12}\\ \sigma^{13}\end{bmatrix} = \frac{E\epsilon_{11}}{(1+\alpha^2\rho^2)^2}\begin{bmatrix}1\\ \alpha\left[-\xi^2\, sin\left(\theta(\xi^1)\right) - \xi^3 cos\left(\theta(\xi^1)\right)\right]\\ \alpha\left[\xi^2 cos\left(\theta(\xi^1)\right) - \xi^3\, sin\left(\theta(\xi^1)\right)\right]\end{bmatrix} \tag{18}$$

Some interesting observation can be drawn from the above equation:

1. Except for the centroid, the normal stress component, σ^{11}, is smaller at every point of the cross section in the development presented here than it would be in the existing publications, given the same axial strain ε_{11}. The difference is, of course, caused by the term $(1+\alpha^2\rho^2)^2$ present in the denominator, which is always grater than 1. And that difference increases with the distance ρ from the

centroid. That may be viewed as immaterial for the existing stability analyses, because they operate with the axial force *N*, and the strain ε_{11} is never a part of analysis. But, as seen subsequently, that has an effect on the bending stiffness as well, which is important from the stability point of view.

2. The resultant of the two shear components (the resultant shear stress) is tangent to the circle of radius ρ, which is the projection of the helix on the plane of the cross section. That resultant shear is

$$\tau = \frac{E\epsilon_{11}}{(1+\alpha^2\rho^2)^2}[\alpha^2((\xi^2)^2 + (\xi^3)^2)]^{1/2} = \frac{E\epsilon_{11}\alpha\rho}{(1+\alpha^2\rho^2)^2} \qquad (19)$$

   Its value is clearly constant for $\rho=const$.

3. Because of the shear stresses, the purely axial deformation of the pre-twisted bar is associated with the presence of the resultant axial force *N,* and the resultant torsional moment *T.* In view of eqs. (18) and (19) they are

$$N = \int_A \frac{E\epsilon_{11}}{(1+\alpha^2\rho^2)^2} dA = C_1\epsilon_{11} \qquad (20a)$$

$$T = \int_A \frac{E\epsilon_{11}\alpha\rho^2}{(1+\alpha^2\rho^2)^2} dA = C_2\epsilon_{11} \qquad (20b)$$

   with the meaning of the constants C_1 and C_2 clearly identifiable based on the above equations. These last formulas are analogous to those well established in the area of wire rope mechanics (Raoof and Kraincanic, 1995) although the constants C_1 and C_2 are, obviously, different there. The reason is the helical geometry that the wire ropes and pre-twisted bars share.

   It is noted that this purely axial deformation, leading to the existence of the torsional moment *T* defined in eq. (20b), requires that the rotation about the axis of the bar is prevented at its ends. In fact, that rotation is not a part of the model, so it is prevented everywhere. Thus, *T* should be regarded as internal reaction, much like the shear force in Euler-Bernoulli model of beams. Also like the shear forces in the Euler-Bernoulli model of beams the torque *T* should enter equilibrium equations of the bar.

If the rotation about bar's axis was a part of the model, and if it was not restrained at one end, rotation along the bar would occur to relieve moment *T* everywhere. To investigate the effects of moment *T* the subsequent development will consider both cases: the one in which moment *T* is included and one in which *T=0*.

4. The formula defining moment *T* depends, of course, on the assumed distribution of stresses in the bar. However, some value of *T* has to be present even if other distribution of stresses is assumed. It is so because, at the corner zones, the dominant stress direction is parallel to the corner helix, as was rigorously proven in eqs. (13), (14) and (15).

3. Stability equations in terms of the resultant forces of the bar.

3.1. General equilibrium conditions of arbitrarily shaped three-dimensional bar.

The starting point here are the well-known general equilibrium equations of a three-dimensional (large or small) deformation of a bar that, at least in its current configuration, is assumed to be curved. For slender bars it is typically assumed that the stress resultants in the bar consist of the resultant force vector ***F*** (applied at the centroids) and the resultant couple vector ***M***. Given that the Euler-Bernoulli assumptions are adopted in this work and the cross sections are orthogonal to the deformed line formed by the centroids, an orthonormal vector basis $\boldsymbol{s}_K$ can be attached to each point of the centroidal line, with $\boldsymbol{s}_1$ being tangent to that line and $\boldsymbol{s}_2$, $\boldsymbol{s}_3$ located in the plane of the cross section. Furthermore, assuming that the centroidal line is parametrized by its arc length l^1 and that distances in the plane of the cross section, measured from the centroids along $\boldsymbol{s}_2$ and $\boldsymbol{s}_3$, are l^2 and l^3, one has $\boldsymbol{s}_K = \partial \boldsymbol{r}/\partial l^1$, where ***r*** is the position vector.

The vector form of the bar equilibrium equations are then as follows (Wempner, 1973)

$$\boldsymbol{F}_{,1}+\boldsymbol{p}=\boldsymbol{0} \tag{21a}$$

$$\boldsymbol{M}_{,1}+\boldsymbol{s}_1\times\boldsymbol{F}+\boldsymbol{m}=\boldsymbol{0} \tag{21b}$$

Where $\boldsymbol{p}$ is external load vector, $\boldsymbol{m}$ is external moment vector, symbol × signifies the operation of cross product, and the differentiation is with respect l^1. The component form of the above vector equations, written relative to the vector basis $\boldsymbol{s}_K$, is (Wempner, 1973):

$$F^1{}_{,1}-\kappa_2F^2-\kappa_3F^3+p^1=0 \tag{22a}$$

$$F^2{}_{,1}+\kappa_2F^1-\kappa_1F^3+p^2=0 \tag{22b}$$

$$F^3{}_{,1}+\kappa_3F^1+\kappa_1F^2+p^3=0 \tag{22c}$$

$$M^1{}_{,1}-\kappa_2M^2-\kappa_3M^3+m^1=0 \tag{22d}$$

$$M^2{}_{,1}+\kappa_2M^1-\kappa_1M^3-F^3+m^2=0 \tag{22e}$$

$$M^3{}_{,1}+\kappa_3M^1+\kappa_1M^2+F^2+m^3=0 \tag{22f}$$

where

$$\kappa_1=\boldsymbol{s}_{2,1}\cdot\boldsymbol{s}_3=-\boldsymbol{s}_{3,1}\cdot\boldsymbol{s}_2 \tag{23a}$$

$$\kappa_2=\boldsymbol{s}_{1,1}\cdot\boldsymbol{s}_2=-\boldsymbol{s}_{2,1}\cdot\boldsymbol{s}_1 \tag{23b}$$

$$\kappa_3=\boldsymbol{s}_{1,1}\cdot\boldsymbol{s}_3=-\boldsymbol{s}_{3,1}\cdot\boldsymbol{s}_1 \tag{23c}$$

with κ_1 representing "torsion" of the centroidal curve whereas κ_2 and κ_3 are its "curvatures" in the planes defined by vectors $\boldsymbol{s}_1$-$\boldsymbol{s}_2$ and vectors $\boldsymbol{s}_1$-$\boldsymbol{s}_3$, respectively. The formulas of eqs. (23a,b,c) are akin to the well-known Frenet formulas (Banchoff and Lovett, 2022) except in the Frenet formulas specially defined vectors $\boldsymbol{s}_K$ are used. The Frenet-Serret equations are in essence the concept of relating derivatives of orthogonal vectors along parametrized curves. The curve that we are considering in this instance would be the curvature generated by the deflected buckling shape of the post buckled column.

As is well known, the equations defining stability problems are those describing small variations of the problem's variables superposed on their pre-existing finite state. In the context of the stability problem of a straight bar considered here, these equations are similar to those describing small variations in κ_K, F^K and M^K when an *"infinitesimally small"* variations of the load $\boldsymbol{p}$ and/or $\boldsymbol{m}$ are specified. As those changes must occur while satisfying the equilibrium equations specified in eqs. (22a-f), the changes in κ_K, F^K and M^K must satisfy the "linearized" forms of eqs. (22a-f):

$$\Delta F^1{}_{,1} - \kappa_2 \Delta F^2 - \kappa_3 \Delta F^3 - \Delta\kappa_2 F^2 - \Delta\kappa_3 F^3 + \Delta p^1 = 0 \qquad (24a)$$

$$\Delta F^2{}_{,1} + \kappa_2 \Delta F^1 - \kappa_1 \Delta F^3 + \Delta\kappa_2 F^1 - \Delta\kappa_1 F^3 + \Delta p^2 = 0 \qquad (24b)$$

$$\Delta F^3{}_{,1} + \kappa_3 \Delta F^1 + \kappa_1 \Delta F^2 + \Delta\kappa_3 F^1 + \Delta\kappa_1 F^2 + \Delta p^3 = 0 \qquad (24c)$$

$$\Delta M^1{}_{,1} - \kappa_2 \Delta M^2 - \kappa_3 \Delta M^3 - \Delta\kappa_2 M^2 - \Delta\kappa_3 M^3 + \Delta m^1 = 0 \qquad (24d)$$

$$\Delta M^2{}_{,1} + \kappa_2 \Delta M^1 - \kappa_1 \Delta M^3 + \Delta\kappa_2 M^1 - \Delta\kappa_1 M^3 - \Delta F^3 + \Delta m^2 = 0 \qquad (24e)$$

$$\Delta M^3{}_{,1} + \kappa_{3\Delta} M^1 + \kappa_1 \Delta M^2 + \Delta\kappa_3 M^1 + \Delta\kappa_1 M^2 + \Delta F^2 + \Delta m^3 = 0 \qquad (24f)$$

with Δ representing a small change in the variable that follows. However, in the stability problem considered herein the only external load is *N,* so $\boldsymbol{p} = \boldsymbol{m} = \boldsymbol{0}$ and $\Delta p^K = \Delta m^K = 0$.

3.2. Equilibrium of the buckled, pre-twisted straight bar.

To extract the equations relevant to the buckling problem of the pre-twisted straight bar it is first noted that the axial load can be defined by the axial deformation ε_{11} or, equivalently, by *N* present in eqs. (20a,b). The problem is to find what value of that load may be associated with equilibrium configuration other than the axially stressed straight configuration. That straight configuration is parametrized by the arc length $x^1 = \xi^1 = l^1$, and it is possible to assume $\boldsymbol{s}_k = \boldsymbol{e}_K$, which implies that $\kappa_K = 0,\ K = 1,2,3$. The non-vanishing initial resultant forces are only $F^1 = N$ and $M^1 = T$ defined in eqs. (20a,b), which are constant assuming a constant rate of twist α. With that specification eqs. (24a) and (24d) are identically satisfied, and the remaining four equations are:

$$\Delta F^2{}_{,1} + \Delta\kappa_2 N = 0 \tag{25b}$$

$$\Delta F^3{}_{,1} + \Delta\kappa_3 N = 0 \tag{25c}$$

$$\Delta M^2{}_{,1} + \Delta\kappa_2 T - \Delta F^3 = (\Delta M^2 + \Delta u^2{}_{,1}\, T)_{,1} - \Delta F^3 = 0 \tag{25e}$$

$$\Delta M^3{}_{,1} + \Delta\kappa_3 T + \Delta F^2 = (\Delta M^3 + \Delta u^3{}_{,1}\, T)_{,1} + \Delta F^2 = 0 \tag{25f}$$

where the second form of eqs. (25e) and (25f) was possible because *T=const*. This second form clearly shows that the equilibrium of the buckled configuration of the bar is satisfied by the "effective bending moments" that consists of the moments due to bending combined with the projection of the torque *T*.

Differentiating eq. (25f) with respect to x^1 and combining it with eq. (25b) and eqs. (20a,b), and performing the same operations on eqs. (25c) and (25e), the following two equations are obtained

$$\Delta M^2{}_{,11} + \Delta\kappa_{2,1}\, T + \Delta\kappa_3 N = 0 \tag{26e}$$

$$\Delta M^3{}_{,11} + \Delta\kappa_{3,1}\, T - \Delta\kappa_2 N = 0 \tag{26f}$$

With another use of eqs. (20a,b), the above equations can be given the following, equivalent form

$$\Delta M^2{}_{,11} + \Delta\kappa_{2,1}\, \beta N + \Delta\kappa_3 N = 0 \tag{27e}$$

$$\Delta M^3{}_{,11} + \Delta\kappa_{3,1}\, \beta N - \Delta\kappa_2 N = 0 \tag{27f}$$

in which *N* is the critical axial force sought and $\beta = C_2/C_1$. The second terms in this last set of two equations are *never* included in the existing analyses of stability of pre-twisted bars. While in this specific form of those equations the remaining two terms are identical as in all previous formulations, in the next subsection it will be shown that the first terms of eqs. (27e,f) contain additional essential differences.

3.2. Constitutive equations for the linearized bending moments.

For the straight pre-buckled configuration of the bar $\Delta\kappa_2$ and $\Delta\kappa_3$ are defined in the usual way

$$\Delta\kappa_2 = \Delta u^2{}_{,11} \tag{28a}$$

$$\Delta\kappa_3 = \Delta u^3{}_{,11} \tag{28b}$$

where Δu^2 and Δu^3 are small displacements of the centroidal line in $\boldsymbol{e}_2$ and $\boldsymbol{e}_3$ direction, respectively. The strains ε_{11} at every point of the cross section are also defined in the usual way to be

$$\Delta\varepsilon_{11} = -\Delta\kappa_2 x^2 - \Delta\kappa_3 x^3 \tag{29}$$

However, the stresses caused by bending still need to satisfy traction-free conditions on the side surfaces of the column and need to be modified as discussed in Section 2.2. As a result

$$\Delta\sigma^{11} = \frac{E\Delta\epsilon_{11}}{(1+\alpha^2\rho^2)^2} = -\frac{E}{(1+\alpha^2\rho^2)^2}(\Delta\kappa_2 x^2 + \Delta\kappa_3 x^3) \tag{30}$$

The corresponding bending moments are

$$\Delta M^2 = \int_A x^3 \Delta\sigma^{11} dA = -E\bar{I}_{23}\Delta\kappa_2 - E\bar{I}_2\Delta\kappa_3 \tag{31a}$$

$$\Delta M^3 = -\int_A x^2 \Delta\sigma^{11} dA = E\bar{I}_3\Delta\kappa_2 + E\bar{I}_{23}\Delta\kappa_3 \tag{31b}$$

where,

$$\bar{I}_2 = \int_A \frac{(x^3)^2}{(1+\alpha^2\rho^2)^2} dA \tag{32a}$$

$$\bar{I}_3 = \int_A \frac{(x^2)^2}{(1+\alpha^2\rho^2)^2} dA \tag{32b}$$

$$\bar{I}_{23} = \int_A \frac{x^2 x^3}{(1+\alpha^2\rho^2)^2} dA \tag{32c}$$

are weighted moments and products of inertia. The presence of the weight function $1/(1+\alpha^2\rho^2)^2$ in the above equaions, lowers the bending stiffness of the pre-twisted bars, compared to those in the existing papers on the subject, and is expected to lower their buckling force *N*. That effect will be examined numerically in Section 6.

Some comments are perhaps in order at that point:

1. It is interesting to note that the same bending stiffness would be obtained for a special prismatic functionally graded bar in which the Young's modulus is $E(\rho) = \frac{E}{(1+\alpha^2\rho^2)^2}$, with *E* being its value at the cross section centroid.
2. The logic leading to the weight function of the form $1/(1+\alpha^2\rho^2)^2$ is the same as the one that leads to eq. (20b) for torque *T* and is related to the assumed distribution of stresses. So, as remarked in Section 2.3, a different distribution of stresses would cause a different reduction in bending stiffness, but some reduction will always be present.

3.3. Differential equations of bars stability problem and their weak formulation.

Combining eqs. (27e,f), (28a,b) and (31a,b) leads to the following differential equations describing the problem in terms of displacements

$$E(\bar{I}_{23}\Delta u^2{}_{,11} + \bar{I}_2\Delta u^3{}_{,11})_{,11} - (\beta\Delta u^2{}_{,111} + \Delta u^3{}_{,11})N = 0 \qquad (33e)$$

$$E(\bar{I}_3\Delta u^2{}_{,11} + \bar{I}_{23}\Delta u^3{}_{,11})_{,11} - (-\beta\Delta u^3{}_{,111} + \Delta u^2{}_{,11})N = 0 \qquad (33f)$$

in which *N* is the critical axial force sought and $\beta = C_2/C_1$. As always in the problems of stability analysis, this is an eigenvalue problem with *N* being the eigenvalue. The displacements u^2 and u^3 couple these two equations together, if the bar is pre-twisted.

In the remainder of this section a weak formulation of the problem is developed. There are several reasons for this development. One is that it will facilitate a comparison with the energy formulation of the stability problem for pre-twisted bars presented in the next section. The second reason is that with such development it is easier to see which

kinematic and kinetic boundary conditions are “dual”, and what possible boundary conditions could be imposed. Finally, the weak formulation presented here will be the basis for the finite element numerical solution for some illustrative problems.

Although the goal is to develop the weak formulation for eqs. (33e,f), it is bit more transparent to start with eqs. (26e,f) whose weak form is

$$\int_0^L [\delta u^2(\Delta M^3{}_{,11} + \Delta\kappa_{3,1}\, T - \Delta u^2{}_{,11}\, N)$$

$$- \delta u^3(\Delta M^2{}_{,11} + \Delta\kappa_{2,1}\, T + \Delta u^3{}_{,11}\, N)]dx^1 \qquad (34)$$

and it has to be fulfilled for any test functions δu^2, δu^3 which, as is well known, need to fulfill the same kinematic restrictions as u^2 and u^3, respectively. The negative sign in from of δu^3 was chosen based on the physical arguments having to do with the sign in front of F^3 in eq. (25e) (from a formal, mathematical point of view that sign is immaterial). In view of eqs. (28a,b) and of the fact that *T=const* (with *α=const),* integration by parts leads to the following form of the above equation

$$[\delta u^3(-(\Delta M^2 + \Delta u^2{}_{,1}\, T)_{,1} - \Delta u^3{}_{,1}\, N)]_0^L + [\delta u^3{}_{,1}\,(\Delta M^2 + \Delta u^2{}_{,1}\, T)]_0^L$$

$$+[\delta u^2((M^3 + \Delta u^3{}_{,1}\, T)_{,1} - \Delta u^2{}_{,1}\, N)]_0^L - [\delta u^2{}_{,1}\,(M^3 + \Delta u^3{}_{,1}\, T)]_0^L$$

$$+ \int_0^L [-\delta u^3{}_{,11}\,(\Delta M^2 + \Delta u^2{}_{,1}\, T) + \delta u^3{}_{,1}\, \Delta u^3{}_{,1}\, N +$$

$$\delta u^2{}_{,11}\,(\Delta M^3 + \Delta u^3{}_{,1}\, T) + \delta u^2{}_{,1}\, \Delta u^2{}_{,1}\, N]dx^1 = 0 \qquad (35)$$

This equation clearly shows that the following boundary conditions may be considered at either end of the bar in analysis of stability:

$$\Delta u^2 = 0 \quad \text{or} \quad \Delta S^2 = -(M^3 + \Delta u^3{}_{,1}\, T)_{,1} + \Delta u^2{}_{,1}\, N = \Delta F^2 + \Delta u^2{}_{,1}\, N = 0 \qquad (36a)$$

$$\Delta u^3 = 0 \quad \text{or} \quad \Delta S^3 = (\Delta M^2 + \Delta u^2{}_{,1}\, T)_{,1} + \Delta u^3{}_{,1}\, N = \Delta F^3 + \Delta u^3{}_{,1}\, N = 0 \qquad (36b)$$

$$\Delta u^2{}_{,1} = 0 \quad \text{or} \quad \Delta M^3 + \Delta u^3{}_{,1}\, T = 0 \tag{36c}$$

$$\Delta u^3{}_{,1} = 0 \quad \text{or} \quad \Delta M^2 + \Delta u^2{}_{,1}\, T = 0 \tag{36d}$$

The far right formulas in the first two of the above equations are justified based on eqs. (25e,f) and are provided here to elucidate the meaning of ΔS^2 and ΔS^3. In Fig. 2 the resultant forces acting on a section of the buckled bar projected on the x^1-x^2 plane are shown. As clearly follows from eq. (36a) and from that figure, for infinitesimally small Δu^2, ΔS^2 is the component of the resultant force parallel to the global axis x^2, which is the force "work-conjugate" with δu^2. That is the way it should be in the well-constructed weak form in mechanics. Similar figure and identical interpretation is, of course, valid for ΔS^3.

It is also important to note that the boundary condition for moments involves the same "effective moments" as those discussed in connection with eq. (25e,f). In addition, the illustration very similar to that presented in Fig. 2 for the shear force can be drawn to explain the meaning of these effective moments.

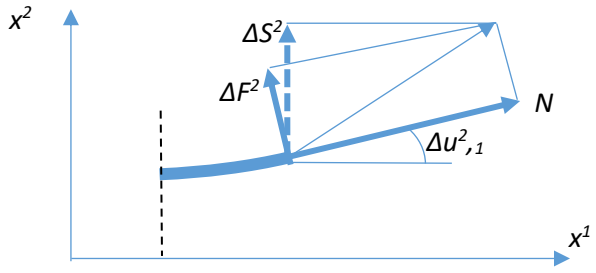

Fig. 2. Internal forces in x^1-x^2 plane. Interpretation of ΔS^2.

Considering the boundary conditions of eqs. (36a-d), the weak formulation applicable in analysis of the pre-twisted columns discussed here involves only the integral part of eq. (35). When the constitutive eqs. (31a, b) are inserted into eq. (35), and the curvatures are expressed in terms of Δu^2 and Δu^3 as specified in eqs. (28a,b), the following matrix form of the weak formulation results

$$\int_0^L \begin{bmatrix} \delta u^2{}_{,1} \\ \delta u^2{}_{,11} \\ \delta u^3{}_{,1} \\ \delta u^3{}_{,11} \end{bmatrix}^T \left\{ \begin{bmatrix} 0 & 0 & 0 & 0 \\ 0 & \bar{I}_3 & 0 & \bar{I}_{23} \\ 0 & 0 & 0 & 0 \\ 0 & \bar{I}_{23} & 0 & \bar{I}_2 \end{bmatrix} + \mathrm{N} \begin{bmatrix} 1 & 0 & 0 & 0 \\ 0 & 0 & \beta & 0 \\ 0 & 0 & 1 & 0 \\ -\beta & 0 & 0 & 0 \end{bmatrix} \right\} \begin{bmatrix} \Delta u^2{}_{,1} \\ \Delta u^2{}_{,11} \\ \Delta u^3{}_{,1} \\ \Delta u^3{}_{,11} \end{bmatrix} dx^1 = 0 \qquad (37)$$

This form will be used to solve the problem numerically employing the finite element method. It is noted, however, that in eq. (37) the matrix multiplying *N*, is not symmetric. It is possible that this will lead to complex values of the buckling loads *N*. Still, eq. (37) will be used in numerical examination of that possibility.

In the next section, a different weak formulation based on structural mechanics equilibrium will be developed in which the lack of symmetry should be weaker. However, for ultimate validation of the proposed approach, in Section 4, stability equations which accounts for the modifications proposed in this work, will be developed based on linearization of the nonlinear, three-dimensional continuum mechanics equations.

As readily discerned, the presented development has been consistently using the convention that the positive components of the resultant forces F^K and resultant moments M^K are represented by vectors aligned with $\boldsymbol{s}_K$, where $\boldsymbol{s}_1$ is unit and orthogonal to the cross section, (cf. eqs. (22-23)). Given that $F^1=N$, that convention specifies the positive *N* in the above equation to be tension. Furthermore, for $\alpha = \Theta_{,1} > 0$, the positive *N* results in *T* which, vectorially, is positive when it is also aligned with vector s_1, as assumed in the development of the preceding **e**quations. As columns buckle only

under compressive force, the sign preceding *N* in eq. (37) should be changed to obtain a positive value of the buckling load.

3.4. Alternative weak formulation based on structural mechanics equations.

Splitting the torsional moment *T* in eq. (34) into two equal contributions, integrating the first one by parts two times and the second only one time, and following logic similar to the one of the previous section the following weak formulation is deduced

$$\int_0^L \begin{bmatrix} \delta u^2{}_{,1} \\ \delta u^2{}_{,11} \\ \delta u^3{}_{,1} \\ \delta u^3{}_{,11} \end{bmatrix}^T \left\{ \begin{bmatrix} 0 & 0 & 0 & 0 \\ 0 & \bar{I}_3 & 0 & \bar{I}_{23} \\ 0 & 0 & 0 & 0 \\ 0 & \bar{I}_{23} & 0 & \bar{I}_2 \end{bmatrix} + \mathrm{N} \begin{bmatrix} 1 & 0 & 0 & -\frac{\beta}{2} \\ 0 & 0 & \frac{\beta}{2} & 0 \\ 0 & \frac{\beta}{2} & 1 & 0 \\ -\frac{\beta}{2} & 0 & 0 & 0 \end{bmatrix} \right\} \begin{bmatrix} \Delta u^2{}_{,1} \\ \Delta u^2{}_{,11} \\ \Delta u^3{}_{,1} \\ \Delta u^3{}_{,11} \end{bmatrix} dx^1$$

$$+ N\beta \frac{1}{2} [\delta u^2{}_{,1} \Delta u^3{}_{,1} - \delta u^3{}_{,1} \Delta u^2{}_{,1}]_0^L = 0 \qquad (38)$$

In the process of deriving the above formula it has been assumed that the boundary conditions specified in eqs. (36a-d) should still be adopted. In particular, the moment boundary conditions should include the entire torque *T*, not only half of it, as only then the physical interpretation of those conditions is acceptable. This issue is elucidated in the preceding section in the discussion of the moment boundary conditions.

The integral part of the formulation presented in eq. (38) is symmetric, but the boundary contributions are not. So, overall, the formulation is still non-symmetric. It is hoped, however, that confining the non-symmetric term to the domain boundaries will have less severe effect on analysis. This too will be examined numerically.

4. Stability of pre-twisted bars based on three-dimensional potential energy.

4.1. Modified potential energy of the problem.

A variational approach based on three-dimensional continuum mechanics will be pursued in this section. In general, this approach leads to a symmetric formulation that will serve to verify the results of Section 3. This time the starting point is nonlinear, three-dimensional version of potential energy into which the kinematic assumption of the bar, and the modifications discussed in Section 2 associated with the pre-twisted geometry of the bar, are introduced. Then the problem is linearized to obtain the variational equations of buckling. The formulation of Section 3 was also based on linearization of the nonlinear equations, but the nonlinearity was confined to the centroidal axis of the bar. In this Section the three-dimensional variational equations are used, and they are nonlinear in the entire volume of the bar. That is why some differences are expected between those two formulations of the problem.

The first variation of the potential energy in nonlinear problems has the following form

$$\delta\mathcal{U} = \int_{\Omega} \delta\boldsymbol{E}:\boldsymbol{S}d\Omega - \Sigma\delta\boldsymbol{u}\cdot\boldsymbol{P} = 0 \tag{39}$$

where symbol δ denotes a small variation in the following quantity, Ω is the volume of the bar, $\boldsymbol{E}$ is Cauchy-Green strain tensor, $\boldsymbol{S}$ the 2nd Piola-Kirchhoff stress tensor and ":" represents their full contraction (inner product) (Malvern, 1969). The displacement $\delta\boldsymbol{u}$ multiplied by the force $\boldsymbol{P}$ under the summation sign symbolically represents the work of external load. The Piola-Kirkoff stress tensor has a direct relation to the green Cauchy strain tensor. Traditional stress tensors such as the Cauchy stress tensor, represent stress in a deformed configuration, which relates traction to the normal vector of the surface. The Piola-Kirchhoff is effectively the 3-d representation of engineering stress where the force applied to a member is applied over the undeformed area. This is useful in the formulation as we do not explicitly know the complete deformed configuration, so it is convenient to express the stress in terms of the undeformed configuration. With

appropriate understanding, eq. (39) is applicable to both the equilibrium state prior to buckling as well as to the state after buckling.

For elastic stability problems and structural engineering applications considered here the deformations can be (and typically are) assumed small, so there is no distinction between the initial and current configuration and the Piola-Kirchhoff stress tensor $\boldsymbol{S}$ can be identified with the Cauchy stress $\boldsymbol{\sigma}$. Additionally, as argued in Section 2, the stress in pre-twisted bars is one-dimensional and has the form of eq. (11). Under this condition eq. (39) takes the form

$$\delta\mathcal{U} = \int_{\Omega} \delta\bar{E}_{11}\bar{\sigma}^{11} d\Omega - \Sigma\delta\boldsymbol{u}\cdot\boldsymbol{P} = 0 \tag{40}$$

where $\delta\bar{E}_{11}$ is the component of the nonlinear strain tensor along the parametric helical ξ^1 line defined as

$$\bar{E}_{11} = \frac{1}{2}\frac{g_{11}-G_{11}}{G_{11}} = \frac{1}{2}\frac{\boldsymbol{r}_{,1}\cdot\boldsymbol{r}_{,1}-\boldsymbol{G}_{11}}{\boldsymbol{G}_{11}} \tag{41}$$

with G_{11} specified in eq. (3b) and $\boldsymbol{r}$ being the position vector of the displaced material points of the bar

$$\boldsymbol{r}(\xi^1,\xi^2,\xi^3) = \boldsymbol{R} + (u^1 - u^2{}_{,1}\,x^2 - u^3{}_{,1}\,x^3)\boldsymbol{e_1} + u^2\boldsymbol{e_2} + u^3\boldsymbol{e_3} \tag{42}$$

As clearly identifiable in the above equations u^1, u^2, u^3 are the displacements of the centroidal axis of the bar which are functions of only ξ^1, whereas x^2 and x^3 are functions of ξ^1 , ξ^2 and ξ^3 (cf. eq.(1)). As a result

$$\boldsymbol{g}_1 = \boldsymbol{r}_{,1} = \boldsymbol{G}_1 + (u^1{}_{,1} - u^2{}_{,11}\,x^2 - u^3{}_{,11}\,x^3 + \alpha u^2{}_{,1}\,x^3 - \alpha u^3{}_{,1}\,x^2)\boldsymbol{e_1} + u^2{}_{,1}\,\boldsymbol{e_2} + u^3{}_{,1}\,\boldsymbol{e_3} \tag{43}$$

$$\delta\bar{E}_{11} = \frac{1}{G_{11}}\,\boldsymbol{r}_{,1}\cdot\delta\boldsymbol{r}_{,1} \tag{44}$$

$$\delta\boldsymbol{r}_{,1} = (\delta u^1{}_{,1} - \delta u^2{}_{,11}\,x^2 - \delta u^3{}_{,11}\,x^3 + \alpha\delta u^2{}_{,1}\,x^3 - \alpha\delta u^3{}_{,1}\,x^2)\boldsymbol{e_1} + \delta u^2{}_{,1}\,\boldsymbol{e_2} + \delta u^3{}_{,1}\,\boldsymbol{e_3} \tag{45}$$

eqs. (41)- (45) describe both the pre-buckling deformation pattern, when $u^2 = u^3 = \delta u^2 = \delta u^3 = 0$, *but* $u^1 \neq 0$ and $\delta u^1 \neq 0$, as well as post-buckling deformation, when $u^1 = const$, but $u^2 \neq 0$, $u^3 \neq 0$ and $\delta u^2 \neq 0$, $\delta u^3 \neq 0$. To detect instability, it is sufficient to consider only small departure from the axially stressed straight pre-buckled configuration, consequently the usual structural mechanics assumptions about the cross section being flat and orthogonal to the deformed centroidal axis are in eq. (42) introduced the way it is done in small deformation theory.

4.2. Variational equation of pre-twisted bars stability.

At the instance of buckling the straight configuration is associated with some strain level $\varepsilon_{11} = const$ and the corresponding stress distribution $\bar{\sigma}^{11} = E\bar{\epsilon}_{11} = \frac{E\epsilon_{11}}{1+\alpha^2\rho^2}$ specified in eq. (17). Due to the distance from the centroid, ρ, present in this formula that stress varies over the cross section. The buckled configuration is described by the transverse displacements of the centroidal line, Δu^2, Δu^3, and variationally tested with arbitrary test functions δu^2, δu^3. Thus, the variational equation describing onset of buckling is obtained by linearization of eq. (40) around the critical straight equilibrium configuration

$$\Delta \int_\Omega \delta\bar{E}_{11}\bar{\sigma}^{11}\, d\Omega = 0 \tag{46}$$

or

$$\int_\Omega (\delta\bar{E}_{11}\Delta\bar{\sigma}^{11} + \Delta\delta\bar{E}_{11}\bar{\sigma}^{11})\, d\Omega = 0 \tag{47}$$

This last step between eq. (46) and eq. (47) parallels the transition from eqs. (22) to eqs. (24) in Section 3.1, with the first term in eq. (47) equivalent to the increments of the resultant forces and the second analogous to the increments of the curvatures present in eqs. (24).

To transform eq. (47) to one that describes the buckled configuration of the bar the stressed and straight configuration at the moment of buckling is considered. At that

state $u^2 = u^3 = 0$, $u^1 = const$ is assumed small and associated with ε_{11} (implying $R \approx R + u^1$, which is valid in most applications), and the buckled configuration is described by superposed small displacements Δu^2 and Δu^3. The only relevant test functions are δu^2 and δu^3 which, together with Δu^2 and Δu^3, should comply with kinematics specified in eq. (42) (cf. eq. (45)). This leads to the following sequence of expressions

$$\delta \boldsymbol{r}_{,1} = \begin{bmatrix} \alpha x^3 & -x^2 & -\alpha x^2 & -x^3 \\ \mathbf{1} & \mathbf{0} & \mathbf{0} & \mathbf{0} \\ \mathbf{0} & \mathbf{0} & \mathbf{1} & \mathbf{0} \end{bmatrix} \begin{bmatrix} \delta u^2{}_{,1} \\ \delta u^2{}_{,11} \\ \delta u^3{}_{,1} \\ \delta u^3{}_{,11} \end{bmatrix} = \boldsymbol{M} \begin{bmatrix} \delta u^2{}_{,1} \\ \delta u^2{}_{,11} \\ \delta u^3{}_{,1} \\ \delta u^3{}_{,11} \end{bmatrix} \tag{48}$$

$$\delta \bar{E}_{11} = \frac{1}{G_{11}} \boldsymbol{R}_{,1} \cdot \delta \boldsymbol{r}_{,1} = \frac{1}{G_{11}} \begin{bmatrix} \mathbf{1} \\ -\alpha \boldsymbol{x^3} \\ \alpha \boldsymbol{x^2} \end{bmatrix}^{\boldsymbol{T}} \boldsymbol{M} \begin{bmatrix} \delta u^2{}_{,1} \\ \delta u^2{}_{,11} \\ \delta u^3{}_{,1} \\ \delta u^3{}_{,11} \end{bmatrix} =$$

$$= \frac{1}{1+\alpha^2\rho^2} \begin{bmatrix} 0 & -x^2 & 0 & -x^3 \end{bmatrix} \begin{bmatrix} \delta u^2{}_{,1} \\ \delta u^2{}_{,11} \\ \delta u^3{}_{,1} \\ \delta u^3{}_{,11} \end{bmatrix} = \frac{1}{1+\alpha^2\rho^2} \boldsymbol{B} \begin{bmatrix} \delta u^2{}_{,1} \\ \delta u^2{}_{,11} \\ \delta u^3{}_{,1} \\ \delta u^3{}_{,11} \end{bmatrix} \tag{49}$$

The strain increment $\Delta \bar{E}_{11}$ is defined by eq. (49) in which the symbol δ is replaced by Δ, thus

$$\Delta \bar{\sigma}^{11} = E \, \Delta \bar{E}_{11} = \frac{E}{1+\alpha^2\rho^2} \boldsymbol{B} \begin{bmatrix} \Delta u^2{}_{,1} \\ \Delta u^2{}_{,11} \\ \Delta u^3{}_{,1} \\ \Delta u^3{}_{,11} \end{bmatrix} \tag{50}$$

Furthermore, considering eq. (44) and the fact that $\Delta \boldsymbol{r}_{,1}$ is specified by eq. (48) in which, again, the symbol δ is replaced by Δ, one has

$$\Delta\delta\bar{E}_{11} = \frac{1}{G_{11}}\,\boldsymbol{\delta r}_{,1}\cdot\Delta\boldsymbol{r}_{,1} = \begin{bmatrix}\delta u^2{}_{,1}\\ \delta u^2{}_{,11}\\ \delta u^3{}_{,1}\\ \delta u^3{}_{,11}\end{bmatrix}^{\boldsymbol{T}} \left(\frac{1}{1+\alpha^2\rho^2}\boldsymbol{M^T M}\right)\begin{bmatrix}\Delta u^2{}_{,1}\\ \Delta u^2{}_{,11}\\ \Delta u^3{}_{,1}\\ \Delta u^3{}_{,11}\end{bmatrix} \tag{51}$$

Inserting eqs. (17), (49), (50) and (51) into eq. (47), the following variational description of pre-twisted bar stability is obtained

$$\int_0^L \begin{bmatrix}\delta u^2{}_{,1}\\ \delta u^2{}_{,11}\\ \delta u^3{}_{,1}\\ \delta u^3{}_{,11}\end{bmatrix}^{\boldsymbol{T}} \left[\int_A \left(\frac{E}{(1+\alpha^2\rho^2)^2}\boldsymbol{B^T B}\right) dA + \int_A \left(\frac{E\epsilon_{11}}{(1+\alpha^2\rho^2)^2}\boldsymbol{M^T M}\right) dA\right]\begin{bmatrix}\Delta u^2{}_{,1}\\ \Delta u^2{}_{,11}\\ \Delta u^3{}_{,1}\\ \Delta u^3{}_{,11}\end{bmatrix} dx^1 = 0 \tag{52}$$

With matrices ***B*** and ***M*** as Identified in eqs. (48) and (49) the above equation is transformed to a more explicit form:

$$\int_0^L \begin{bmatrix}\delta u^2{}_{,1}\\ \delta u^2{}_{,11}\\ \delta u^3{}_{,1}\\ \delta u^3{}_{,11}\end{bmatrix}^{T} \left\{ E\begin{bmatrix}0 & 0 & 0 & 0\\ 0 & \bar{I}_3 & 0 & \bar{I}_{23}\\ 0 & 0 & 0 & 0\\ 0 & \bar{I}_{23} & 0 & \bar{I}_2\end{bmatrix} + \varepsilon_{11}E\begin{bmatrix}\bar{A}+\alpha^2\bar{I}_2 & -\alpha\bar{I}_{23} & -\alpha^2\bar{I}_{23} & -\alpha\bar{I}_2\\ -\alpha\bar{I}_{23} & \bar{I}_3 & \alpha\bar{I}_3 & \bar{I}_{23}\\ -\alpha^2\bar{I}_{23}^2 & \alpha\bar{I}_3 & \bar{A}+\alpha^2\bar{I}_3 & \alpha\bar{I}_{23}\\ -\alpha\bar{I}_2 & \bar{I}_{23} & \alpha\bar{I}_{23} & \bar{I}_2\end{bmatrix}\right\}\begin{bmatrix}\Delta u^2{}_{,1}\\ \Delta u^2{}_{,11}\\ \Delta u^3{}_{,1}\\ \Delta u^3{}_{,11}\end{bmatrix} dx^1 = 0 \tag{53}$$

The symbols present in this equation, $\bar{I}_2$, $\bar{I}_3$ and $\bar{I}_{23}$, have been used before and are specified in eqs. (32a,b,c). The only new symbol is

$$\bar{A} = \int_A \frac{1}{(1+\alpha^2\rho^2)^2} dA \tag{54}$$

which is the weighted cross section area.

eq. (53) is the variational eigenvalue equation in which ε_{11} is the eigenvalue. It is clear from this equation that the solution of that equation (i.e. the resulting eigenvalue ε_{11}) is independent of the Young modulus E, which can be taken out of it. To specify the critical buckling force compatible with the development pursued in this work, this eigenvalue needs to be inserted into eq. (20a).

4.3. Differential equations and boundary conditions resulting from the three-dimensional variational formulation (Euler-Lagrange equations).

Differential equation of the buckled beam will not be used in this work and is presented here to have a complete description. To obtain the differential equations governing the problem and the associated boundary conditions, the process analogical to that used in Section 3.3 is followed, but it is used in reverse. Only the final result is presented here given that straightforward integrations by parts are the only operations involved. Thus, the two differential equations corresponding to the two independent and arbitrary functions δu^2 and δu^3 are, respectively:

$$\begin{aligned}
&E(\bar{I}_3 \Delta u^2{}_{,11} + \bar{I}_{23} \Delta u^3{}_{,11})_{,11} + \\
&+\varepsilon_{11} E\left(-\alpha \bar{I}_{23} \Delta u^2{}_{,1} + \bar{I}_3 \Delta u^2{}_{,11} + \alpha \bar{I}_3\, \Delta u^3{}_{,1} + \bar{I}_{23} \Delta u^3{}_{,11}\right)_{,11} - \\
&-\varepsilon_{11} E\left(\left(\bar{A} + \alpha^2 \bar{I}_2\right) \Delta u^2{}_{,1} - \alpha \bar{I}_{23} \Delta u^2{}_{,11} - \alpha^2 \bar{I}_{23} \Delta u^3{}_{,1} - \alpha \bar{I}_2\, \Delta u^3{}_{,11}\right)_{,1} = 0
\end{aligned} \tag{55}$$

$$\begin{aligned}
&E(\bar{I}_{23} \Delta u^2{}_{,11} + \bar{I}_2 \Delta u^3{}_{,11})_{,11} + \\
&+\varepsilon_{11} E\left(-\alpha \bar{I}_2\, \Delta u^2{}_{,1} + \bar{I}_{23} \Delta u^2{}_{,11} + \alpha \bar{I}_{23} \Delta u^3{}_{,1} + \bar{I}_2\, \Delta u^3{}_{,11}\right)_{,11} - \\
&-\varepsilon_{11} E\left(-\alpha^2 \bar{I}_{23} \Delta u^2{}_{,1} + \alpha \bar{I}_3 \Delta u^2{}_{,11} + \left(\bar{A} + \alpha^2 \bar{I}_3\right) \Delta u^3{}_{,1} + \alpha \bar{I}_{23} \Delta u^3{}_{,11}\right)_{,1} = 0
\end{aligned} \tag{56}$$

The boundary conditions emerging from the presented variational formulation are;

a). $\Delta u^2 = 0$

or

$$E(\bar{I}_3 \Delta u^2{}_{,11} + \bar{I}_{23} \Delta u^3{}_{,11})_{,1} +$$

$$+\varepsilon_{11} E\left(-\alpha \bar{I}_{23} \Delta u^2{}_{,1} + \bar{I}_3 \Delta u^2{}_{,11} + \alpha \bar{I}_3 \, \Delta u^3{}_{,1} + \bar{I}_{23} \Delta u^3{}_{,11}\right)_{,1} -$$

$$-\varepsilon_{11} E\left(\left(\bar{A} + \alpha^2 \bar{I}_2\right) \Delta u^2{}_{,1} - \alpha \bar{I}_{23} \Delta u^2{}_{,11} - \alpha^2 \bar{I}_{23} \Delta u^3{}_{,1} - \alpha \bar{I}_2 \, \Delta u^3{}_{,11}\right) = 0 \qquad (57a)$$

b) $\Delta u^2{}_{,1} = 0$

or

$$E(\bar{I}_{23} \Delta u^2{}_{,11} + \bar{I}_2 \Delta u^3{}_{,11}) +$$

$$+\varepsilon_{11} E\left(-\alpha \bar{I}_2 \, \Delta u^2{}_{,1} + \bar{I}_{23} \Delta u^2{}_{,11} + \alpha \bar{I}_{23} \Delta u^3{}_{,1} + \bar{I}_2 \, \Delta u^3{}_{,11}\right) = 0 \qquad (57b)$$

c) $\Delta u^3 = 0$

or

$$E(\bar{I}_{23} \Delta u^2{}_{,11} + \bar{I}_2 \Delta u^3{}_{,11})_{,1} +$$

$$+\varepsilon_{11} E\left(-\alpha \bar{I}_2 \, \Delta u^2{}_{,1} + \bar{I}_{23} \Delta u^2{}_{,11} + \alpha \bar{I}_{23} \Delta u^3{}_{,1} + \bar{I}_2 \, \Delta u^3{}_{,11}\right)_{,1} -$$

$$-\varepsilon_{11} E\left(-\alpha^2 \bar{I}_{23} \Delta u^2{}_{,1} + \alpha \bar{I}_3 \Delta u^2{}_{,11} + \left(\bar{A} + \alpha^2 \bar{I}_3\right) \Delta u^3{}_{,1} + \alpha \bar{I}_{23} \Delta u^3{}_{,11}\right) = 0 \qquad (57c)$$

d) $\Delta u^3{}_{,1} = 0$

or

$$E(\bar{I}_{23} \Delta u^2{}_{,11} + \bar{I}_2 \Delta u^3{}_{,11}) +$$

$$+\varepsilon_{11} \mathrm{E}\left(-\alpha \bar{I}_2 \, \Delta u^2{}_{,1} + \bar{I}_{23} \Delta u^2{}_{,11} + \alpha \bar{I}_{23} \Delta u^3{}_{,1} + \bar{I}_2 \, \Delta u^3{}_{,11}\right) = 0 \qquad (57d)$$

As the transverse displacements are energetically paired with the resultant transverse forces and rotations (slopes) with the resultant moments, eqs. (57a) and (57c) define the transverse resultant forces in direction $\boldsymbol{s_2}$ and $\boldsymbol{s_3}$ whereas eqs. (57b) and (57d) resultant moments aligned with vectors $\boldsymbol{s_3}$ and $\boldsymbol{s_2}$, respectively. Particularly revealing is comparison of eqs. (57b) and (57d) with eqs. (36 c,d). They clearly demonstrate that the parts of those equations multiplied by $\varepsilon_{11}E$ are the contribution of the torsional moments which, this time, have been energetically assigned to the moments associated with bending stiffness of the bar. And that has been done without explicit introduction of the torsional moment *T* into the three-dimensional variational formulation of the problem.

5. A critical evaluation of the proposed modifications

The main new aspect of the formulation proposed here is the new directions and different distribution of stresses over the cross-sectional area of the pre-twisted bars. It is based on the requirements that the side boundaries of the bars be free of tractions. While a degree of approximation is involved in how the stresses are proposed to be distributed over the entire cross section one could argue that a more drastic approximation is adopted in the existing formulations. Those formulations assume distributions that are identical as in the prismatic beams and do not satisfy traction boundary conditions on the side faces when the bars are pre-twisted. It is recognized that approximate theories always violate some conditions that the exact solution is supposed to satisfy, but there is no good reason to ignore in the formulation those conditions that can be *satisfied without changing the main aspects of the theory*. With that in mind it is proposed that the effects of the modifications introduced in this work be examined and discussed.

The proposed new direction and distribution of stresses have two main effects. First, it reduces the bending stiffness of the pre-twisted bars, which must change their

behavior. Along with length and material properties – the bending stiffness is the main factor affecting the magnitude of their buckling load. So, it is expected that it will make the columns less stable. Second, if the rotations around the column longitudinal axis are restrained at both ends, tension (or compression) is associated with presence of torsional moment. This is an additional prestressing force, which, just like the axial compressive load, may additionally influence the magnitude of the buckling load. This coupling between the axial and torsional effects is an essential aspect of the wire rope mechanics (Raoof and Kraincanic, 1995). While the rate of twist of wire ropes is significantly higher and that is likely to make such coupling effects more pronounced, this effect should probably be examined in more details in the context of pre-twisted bars.

The most straightforward approach of formulating the problem is perhaps that based on structural analysis of bars, which is an approach employed in all of the existing contributions on their stability. Unfortunately, use of the structural mechanics approach to develop the relevant equations describing stability of pre-twisted columns and incorporating the torsional moment occurring under compression, leads to non-symmetric formulation (eq. (37)). As is well known, lack of symmetry may lead to complex eigenvalues, which would put in doubt their physical significance. In an effort to mitigate the lack of symmetry an alternative weak form has been developed in which the non-symmetric terms are confined only to the boundary contributions (eq. (38)).

If rotation about the longitudinal axis of the bar is not restrained at least at one end, torsional moment must vanish everywhere and $\theta=0$ in eqs. (37) and (38). The mathematical structure of the formulation developed in Section 3 is then symmetric and exactly like in all past formulations. However, the bending stiffness is different and smaller than in the existing publications. So, the buckling load should be reduced as well.

There is an inconsistency in the proposed formulation when $T=0$ is assumed. Physically that would imply that the rotations around the bar axis occur along the length to relieve

torque *T*. Those rotations are not a part of the model, however, and the mechanism by which *T* could be possibly relieved remains unclear. So, introduction of the rotation about bar's axis in the model would be beneficial in this regard. It is also possible that to avoid complex eigenvalues when *T≠0* rotations about the axis of the column should be a part of the model. This rotation could possibly be introduced in a manner similar to the way it is done in dynamic analysis of rotating pre-twisted bars (Sinha, 2007).

The potential difficulties with the formulation based on the structural mechanics approach described earlier, motivated variational path starting with a general, nonlinear, three-dimensional potential energy. This energy was then specialized to include the main conceptual contributions of this work presented in Section 2. As expected, the resulting equations preserve the symmetry of the formulation, but they are also quite a bit more complex. The increased complexity is confined to the part of the equations that is related to prestressing, though - the material response part remains the same as in the developments based on structural mechanics equations (although with modified bending stiffness, of course). This is understandable, because in bar stability equations it is only the prestressing-related part of the equations that comes from linearization of nonlinear kinematic equations, and the kinematic nonlinearity was the only difference between the structural mechanics and variational approaches.

Comparison of eq. (20a) with eqs. (53) and (54) makes it evident that in eq. (53) $\varepsilon_{11} E\bar{A} = N$. Consequently, in the prestressing-related part of eq. (53) everything other than $\bar{A}$ (present in just two locations, which are the same as in eqs. (37) and (38)), must represent β of eqs. (37) and (38), and, thus, torque *T.* But does it variationally, weighing the τ component of the stress specified in eq. (19) differently at different points of the cross section, not after the integration was performed to compute torque *T*, as in the structural mechanics approach. This is the beauty of the variational approach, which always yields equations consistent with the introduced approximations. And it provided a symmetric formulation!

Clearly, formulating the problem in a fixed Cartesian coordinate system is very inconvenient if closed-form solution of some sort is to be pursued (as in eg. Tabarrok et al., 1990), since the weighted moments and product of inertia appearing in eqs. (55) and (56), or eqs. (33e) and (33f), are functions of x^1. In the entirely numerical solution based on the weak formulations adopted here the difference between descriptions based on a fixed Cartesian coordinate system, or the one in which two axes of the system are the rotating principal axes of the cross section, is practically nonexistent. It is restricted to a few additional lines of the computer code.

6. Finite Element Implementation

In this Section some relevant details related to the numerical analysis conducted in the thesis and the development of the associated MATLAB code are presented. This includes development of the discretized equations of various models presented in the thesis and the overall logic of the code.

6.1. Overall Outline of the Approach

The numerical method used in this thesis to solve the governing equations and associated boundary conditions is the finite element method. The version implemented here is using the Galerkin formulation (Reddy,2018). Given that the problem is one-dimensional (1D), the finite element mesh is generated by dividing the length of the bar into *n* equal segments, or finite elements, with *n-1* "nodes" separating those segments and 2 nodes at the boundaries of the bar. The continuous description of the eigenvalue problems discussed in Section 3 and 4 are converted to their discrete versions by representing the functions involved in those formulations by properly selected nodal parameters, or degrees of freedom. Those nodal parameters are used to approximate the functions describing the problem over each of the finite elements, which allows for the evaluation of the weak formulations presented in eqs. (37), (38) and (53) and transforming them into algebraic eigenvalue problems. The resulting eigenvalues define the buckling loads for the considered bars.

6.2. Continuity Requirements, Nodal Degrees of Freedom and Basis Functions.

Considering that in the weak formulations of the problems specified in eqs. (37), (38) and (53) the derivatives of the highest order are second derivatives, the approximations of functions Δu^2 and Δu^3 should be globally C^1-continuous; This implies derivatives of the first order need to be continuous (Bathe 1996, Reddy 2018). Considering that the functions Δu^2 and Δu^3 will be approximated by polynomials and within each element the C^1 continuity is satisfied automatically if they are high enough order. Thus, the global continuity for both Δu^2 and Δu^3can be satisfied by choosing the nodal values of

those functions and the values of their first derivatives as independent nodal parameters at each node. With that choice, within a typical finite element each of those functions is defined by four parameters – two parameters at each boundary of the element. As a result, cubic polynomials, uniquely defined by four independent parameters, can be chosen to approximate Δu^2 and Δu^3 within each element.

To provide specific formulas, consider a generic finite element located between consecutive nodes *I* and *J* and parametrized by $0<\xi<1$ with $\xi = (x - x_I)/L_e$, $L_e = L/n$ and *L* being the length of the bar. This is illustrated in the Fig. 3.

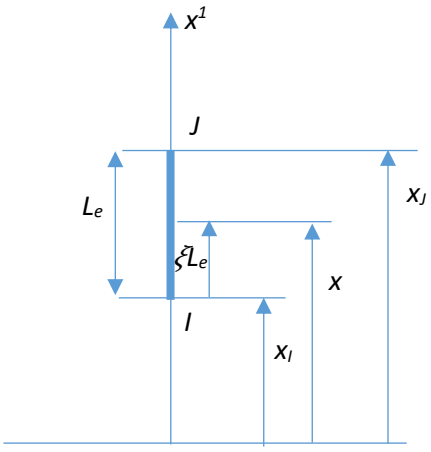

Fig. 3. A generic finite element

With those specifications, and with the following additional notation

$$\Delta u^2{}_{,x}\,(\xi = 0) = \Delta\Theta_I^2,\ \Delta u^2{}_{,x}\,(\xi = 1) = \Delta\Theta_J^2 \tag{58a}$$

$$\Delta u^3{}_{,x}\,(\xi = 0) = \Delta\Theta_I^3,\ \Delta u^3{}_{,x}\,(\xi = 1) = \Delta\Theta_J^3 \tag{58b}$$

the approximation of the functions Δu^2 and Δu^3 is

$$\Delta u^2(\xi) = N_1(\xi)\Delta u_I^2 + N_2(\xi)\Delta\Theta_I^2 + N_3(\xi)\Delta u_J^2 + N_4(\xi)\Delta\Theta_J^2 \qquad (59a)$$

$$\Delta u^3(\xi) = N_1(\xi)\Delta u_I^3 + N_2(\xi)\Delta\Theta_I^3 + N_3(\xi)\Delta u_J^3 + N_4(\xi)\Delta\Theta_J^3 \qquad (59b)$$

with

$$N_1(\xi) = (2 * \xi^3 - 3\xi^2 + 1) \qquad (60a)$$

$$N_2(\xi) = \left(L_e * (\xi^3 - 2\xi^2 + \xi)\right) \qquad (60b)$$

$$N_3(\xi) = (-2\xi^3 + 3\xi^2) \qquad (60c)$$

$$N_4(\xi) = (L_e * (\xi^3 - \xi^2)) \qquad (60d)$$

The test functions δu^2 and δu^3 are approximated using the same basis functions and the same type of degrees of freedom.

6.3. Finite Element Discretization of the Weak Formulations

Approximations of the functions Δu^2 and Δu^3 specified in eqs. (59 a,b), as well as the corresponding approximations of δu^2 and δu^3, are used to transform the weak formulations presented in eqs. (37), (38) and (53) to the corresponding algebraic eigenvalue problems. This process will be presented in one unified framework, which will cover all three equations ((37), (38) and (53), that is). They all can be written as follows:

$$\int_0^L \begin{bmatrix} \delta u^2{}_{,1} \\ \delta u^2{}_{,11} \\ \delta u^3{}_{,1} \\ \delta u^3{}_{,11} \end{bmatrix}^T \{\boldsymbol{D}_M(x^1) + \lambda \boldsymbol{D}_G(x^1)\} \begin{bmatrix} \Delta u^2{}_{,1} \\ \Delta u^2{}_{,11} \\ \Delta u^3{}_{,1} \\ \Delta u^3{}_{,11} \end{bmatrix} dx^1 = 0 \qquad (61)$$

The interpretation of the new notation $\{\boldsymbol{D}_M(x^1) + \lambda \boldsymbol{D}_G(x^1)\}$ is clear when one compares eq. (61) with eq. (37), (38) or (53). In particular the eigenvalue λ is N when eqs. (37) and (38) are implemented and it is ε_{11} when the analysis is based on eq. (53).

Furthermore, dependence of $\boldsymbol{D}_M$ and $\boldsymbol{D}_G$ on $x^1$is specified as a result of x^1-dependent weighted moments of inertia, even though dependence of $\boldsymbol{D}_G$ on x^1 is present only when eq. (53) is used, for the other two formulations $\boldsymbol{D}_G$ is constant.

As noted in the development of eq. (38), the formulation described by eq. (38) requires two additional terms associated with the two ends of the bar.

With the functions involved in the description of the problem approximated as specified above and with the following notations

$$\Delta \boldsymbol{d}_I^T = \{\Delta u_I^2, \Delta\Theta_I^2, \Delta u_I^3, \Delta\Theta_I^3\} \tag{62a}$$

$$\delta \boldsymbol{d}_I^T = \{\delta u_I^2, \delta\Theta_I^2, \delta u_I^3, \delta\Theta_I^3\} \tag{62b}$$

one has

$$\begin{bmatrix} \Delta u^2{}_{,1} \\ \Delta u^2{}_{,11} \\ \Delta u^3{}_{,1} \\ \Delta u^3{}_{,11} \end{bmatrix} = \boldsymbol{B}(\xi) \begin{bmatrix} \Delta \boldsymbol{d}_I \\ \Delta \boldsymbol{d}_J \end{bmatrix} = \tag{63}$$

$$= \frac{1}{(L_e)^2} \begin{bmatrix} L_e N_{1,\xi} & L_e N_{2,\xi} & 0 & 0 & L_e N_{3,\xi} & L_e N_{4,\xi} & 0 & 0 \\ N_{1,\xi\xi} & N_{2,\xi\xi} & 0 & 0 & N_{3,\xi\xi} & N_{4,\xi\xi} & 0 & 0 \\ 0 & 0 & L_e N_{1,\xi} & L_e N_{2,\xi} & 0 & 0 & L_e N_{3,\xi} & L_e N_{4,\xi} \\ 0 & 0 & N_{1,\xi\xi} & N_{1,\xi\xi} & 0 & 0 & N_{3,\xi\xi} & N_{4,\xi\xi} \end{bmatrix} \begin{bmatrix} \Delta \boldsymbol{d}_I \\ \Delta \boldsymbol{d}_J \end{bmatrix}$$

The sequence of steps leading from the weak formulation specified in eq. (61) to algebraic eigenvalue problem are standard and they are listed below:

$$\delta \boldsymbol{d}^T \{\boldsymbol{K}_M + \lambda \boldsymbol{K}_G\} \Delta \boldsymbol{d} = 0 \quad \text{for any } \delta \boldsymbol{d} \tag{64}$$

with

$$\Delta \boldsymbol{d^T} = \left\{ \Delta \boldsymbol{d}_1^T, \quad \Delta \boldsymbol{d}_2^T, \quad \ldots\ldots \Delta \boldsymbol{d}_{n+1}^T, \quad \right\} \tag{65a}$$

$$\delta \boldsymbol{d^T} = \left\{ \delta \boldsymbol{d}_1^T, \quad \delta \boldsymbol{d}_2^T, \quad \ldots\ldots \delta \boldsymbol{d}_{n+1}^T, \quad \right\} \tag{65b}$$

being the global vectors of degrees of freedom and

$$\boldsymbol{K_M} = \boldsymbol{A_{e=1}^{n}} \boldsymbol{k_{Me}} \tag{66a}$$

$$\boldsymbol{K_G} = \boldsymbol{A_{e=1}^{n}} \boldsymbol{k_{Ge}} \tag{66b}$$

In the above equations $\boldsymbol{k_{Me}}$ and $\boldsymbol{k_{Ge}}$ are the element matrices

$$\boldsymbol{k_{Me}} = \int_0^1 \boldsymbol{B}(\xi)^T \boldsymbol{D}_M(\xi) \boldsymbol{B}(\xi) L_e d\xi \tag{67a}$$

$$\boldsymbol{k_{Ge}} = \int_0^1 \boldsymbol{B}(\xi)^T \boldsymbol{D}_G(\xi) \boldsymbol{B}(\xi) L_e d\xi \tag{67b}$$

and the symbol ***A*** signifies the assembly of the *n* element matrices into the global matrices for the problem present in eqs. (64) and (66).

6.4. x^1-Dependent Weighted Moments of Inertia.

As specified in eq. (1)

$$x^2 = \xi^2 \cos\big(\theta(\xi^1)\big) - \xi^3 sin\left(\theta(\xi^1)\right) \tag{68a}$$

$$x^3 = \xi^2 sin\big(\theta(\xi^1)\big) + \xi^3 \cos\big(\theta(\xi^1)\big) \tag{68b}$$

with

$$\theta(\xi^1) = \alpha \xi^1 \tag{69}$$

Thus, for the bar of rectangular cross section of dimension *a x b* one has

$$\bar{I}_2 = \int_A \frac{\left(x^3\right)^2}{(1+\alpha^2\rho^2)^2} dA = \hat{I}_2 cos^2(\theta) + \hat{I}_3 sin^2(\theta) \tag{70a}$$

$$\bar{I}_3 = \int_A \frac{\left(x^2\right)^2}{(1+\alpha^2\rho^2)^2} dA = \hat{I}_2 sin^2(\theta) + \hat{I}_3 sin^2(\theta) \tag{70b}$$

$$\bar{I}_{23} = \int_A \frac{x^2 x^3}{(1+\alpha^2\rho^2)^2} dA = \left(\hat{I}_3 - \hat{I}_2\right) sin\,(\theta) cos(\theta) \tag{70c}$$

Where:

$$\hat{I}_2 = \int_A \frac{\left(\xi^3\right)^2}{(1+\alpha^2\rho^2)^2} dA \tag{71a}$$

$$\hat{I}_3 = \int_A \frac{(\xi^2)^2}{(1+\alpha^2\rho^2)^2} dA \tag{71b}$$

6.5. Numerical Integration.

The integration present in eqs. (67) and (71) is evaluated numerically, using Gauss-Legrange integration (Bathe 1996, Reddy 2018). Four Gauss points have been used in each of the three spatial directions. Thus,

$$\hat{I}_2 = \int_A \frac{(\xi^3)^2}{(1+\alpha^2\rho^2)^2} dA = \sum_{J=1}^{n_G^2} \sum_{K=1}^{n_G^3} W_J W_K \frac{\left(\frac{b}{2}\right)^2 (\zeta_K)^2}{\left(1+\alpha^2\rho_{JK}^2\right)^2} \frac{ab}{4} \tag{72a}$$

$$\hat{I}_3 = \int_A \frac{(\xi^2)^2}{(1+\alpha^2\rho^2)^2} dA = \sum_{J=1}^{n_G^2} \sum_{K=1}^{n_G^3} W_J W_K \frac{\left(\frac{a}{2}\right)^2 (\eta_J)^2}{\left(1+\alpha^2\rho_{JK}^2\right)^2} \frac{ab}{4} \tag{72b}$$

$$\boldsymbol{k_{Me}} = \int_0^1 \boldsymbol{B}(\xi)^T \boldsymbol{D}_M(\xi) \boldsymbol{B}(\xi) L_e d\xi = \sum_{I=1}^{n_G^1} W_I \boldsymbol{B^T}(\xi_I) \boldsymbol{D}_M(\xi_I) \boldsymbol{B}(\xi_I) \frac{L_e}{2} \tag{72c}$$

$$\boldsymbol{k_{Ge}} = \int_0^1 \boldsymbol{B}(\xi)^T \boldsymbol{D}_G(\xi) \boldsymbol{B}(\xi) L_e d\xi = \sum_{I=1}^{n_G^1} W_I \boldsymbol{B^T}(\xi_I) \boldsymbol{D}_G(\xi_I) \boldsymbol{B}(\xi_I) \frac{L_e}{2} \tag{72d}$$

where ξ_I, η_J and ζ_K are the coordinates of the Gauss points with W_I, W_J and W_K being the corresponding weights and

$$\rho_{JK}^2 = \left(\frac{a}{2}\eta_J\right)^2 + \left(\frac{b}{2}\zeta_K\right)^2 \tag{73}$$

The number of Gauss points in the three special directions are denoted by n_G^1, n_G^2 and n_G^3.

6.5. Boundary Conditions and the Final Eigenvalue Problem.

To obtain the final eigenvalue problem describing a specific problem, the boundary conditions of the problem need to be introduced into eq. (64). All of those conditions are kinematic in nature and their introduction amount to removal of the constrained degrees of freedom from the vector $\delta\boldsymbol{d}$ and $\Delta\boldsymbol{d}$ present in eq. (64). This translates into elimination of the corresponding rows and columns from both $\boldsymbol{K_M}$ and $\boldsymbol{K_G}$ and leads to the following reduced final algebraic eigenvalue problem

$$\{\overline{\boldsymbol{K}}_M + \lambda\overline{\boldsymbol{K}}_G\}\Delta\overline{\boldsymbol{d}} = 0 \tag{74}$$

The following rows and columns need to be removed from $\boldsymbol{K}_M$ and $\boldsymbol{K}_G$ for various possible support conditions:

1. For transverse displacement constrained at an end of the bar the column and row multiplied by that displacement in eq. (64) need to be removed in the transformation process leading to eq. (74).
2. For a rotation constrained at an end of the bar the row and column multiplied by that rotation in eq. (64) need to be removed.

The above general rules allow to describe a number of different realistic support conditions. In fact, these support conditions do not need to be confined to the end of the bar – the bar can have displacements and rotations constrained anywhere along its length, and the same general rules will still apply.

6.5. Flow Chart and Computer Program.

The following flow chart depicts the organization of the computer program implementing the theory described in the preceding sections, forks in the chart indicate where new methods were tried and what differentiates them.

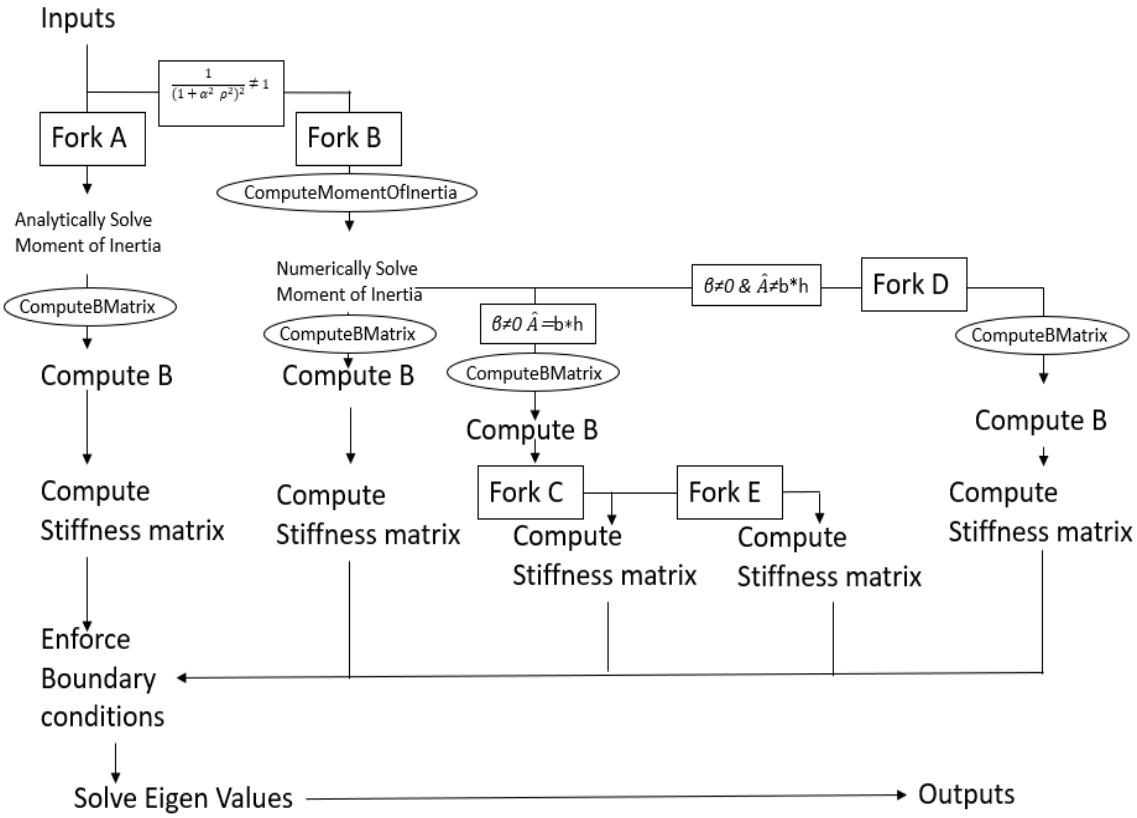

Fig. 4. Code logic flow chart with examining differing approaches

7. Numerical Examples.

In the numerical evaluation of the proposed modifications a bar with the cross section of dimension $\sqrt{2}$ by 1 units of length (resulting in 1:2 ratio of the principal moments of inertia) and 20 units long is considered. A bar of those proportions would normally classify as slender, for which the assumptions made here (of flat and orthogonal to its axis cross sections) are adequate. That ratio of the principal moments of inertia was used in (Tabarrok et al., 1990), and the results presented there for the unmodified theory are used here or the verification. The Young modulus will remain unspecified, so the buckling loads presented here will contain *E* as arbitrary multiplier. When various formulations of the problem are compared the relative pre-twist between the ends of the bar will be varied from *0* to *2π,* and the variation of the smallest buckling load with the magnitude of the total angle of twist will be plotted. This load, irrespectively of what mode it is associated with, is of utmost importance in many practical applications. The following four formulations will be compared:

a) The past formulations in which the moments and product of inertia are not weighed, as proposed here, and β=*0.* (Identified as "Unmodified", cf. eq. (38))
b) The present formulation based on the structural mechanics approach and *β=0.* (Identified as "Model A" and based on eq. (38))
c) The present formulation based on the structural mechanics approach and *β≠0 (T≠0).* (Identified as "Model B" and based on eq. (38))
d) The present formulation based on the potential energy approach. (Identified as "Model C" and based on eq. (53))

All four formulations will be applied to bars with four different support conditions

1) Bar with pin support at both ends, Fig. 3
2) Bar fixed at both ends, Fig. 4
3) Bar fixed at one end and pinned at the other, Fig. 5
4) Bar fixed at one end and free at the other, Fig. 6

The results presented in Figures 3 through 6 are normalized by the smallest buckling load (the weak axis buckling force, that is) for the prismatic (untwisted) bar and for the support conditions considered in the specific Figure. Of course, that normalization eliminates a need for a specific value of the Young modulus.

The method employed in the analysis was the finite element method, with 10 one-dimensional, equal-length, cubic (C^1) finite elements. Given that the smallest buckling load was of main interest that number of elements is adequate. The process involved is quite standard and no details of the finite element implementation are presented here. MATLAB was used as programming environment and its most general eigenvalue solver, allowing for non-symmetric matrices, was employed to find the eigenvalues for the resulting discrete problem.

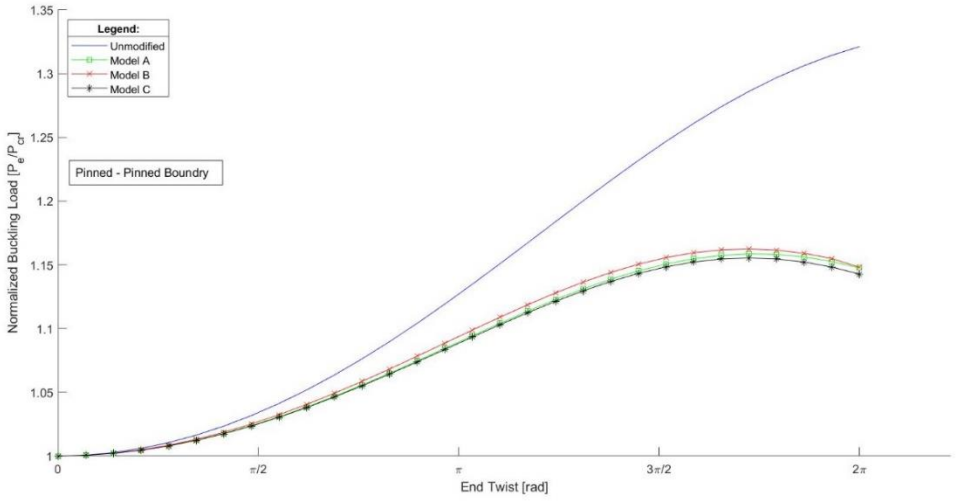

Fig. 5. Buckling load based on modified and unmodified theory for pinned-pinned support of the bar.

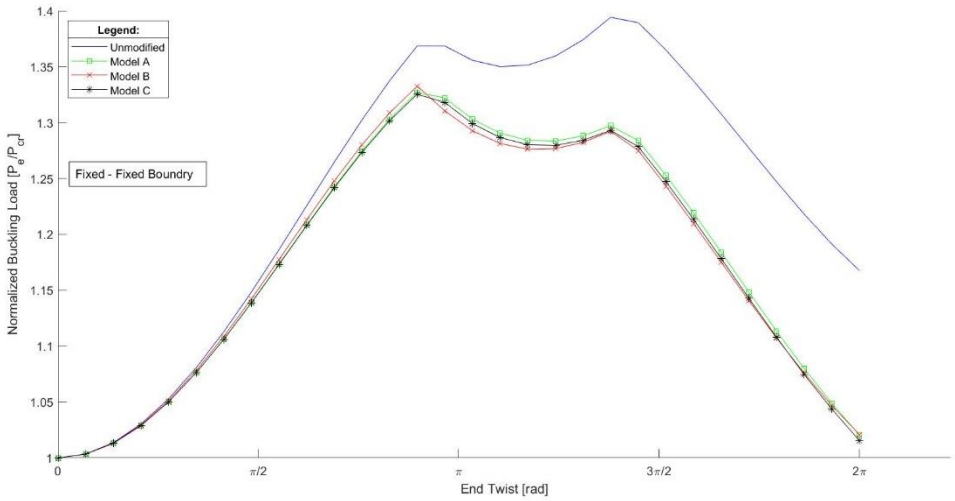

Fig. 6. Buckling load based on modified and unmodified theory for fixed-fixed support of the bar.

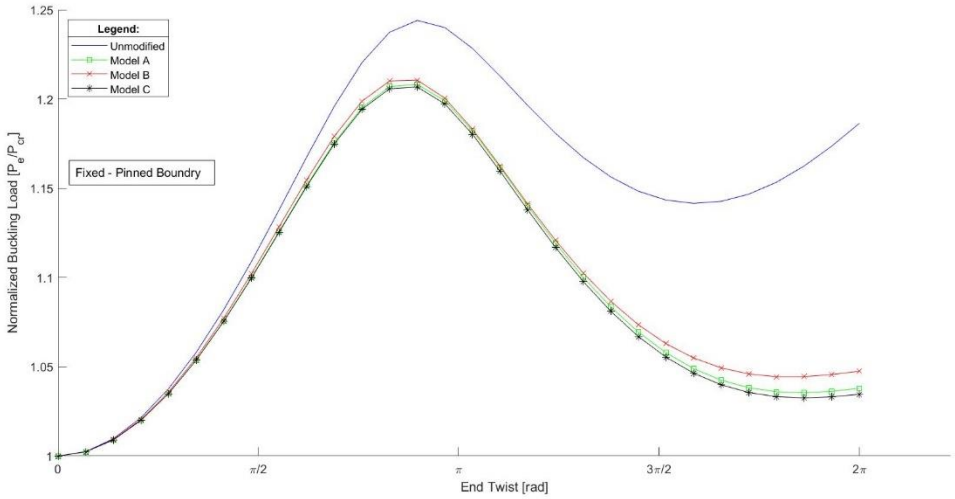

Fig. 7. Buckling load based on modified and unmodified theory for fixed-pinned support of the bar.

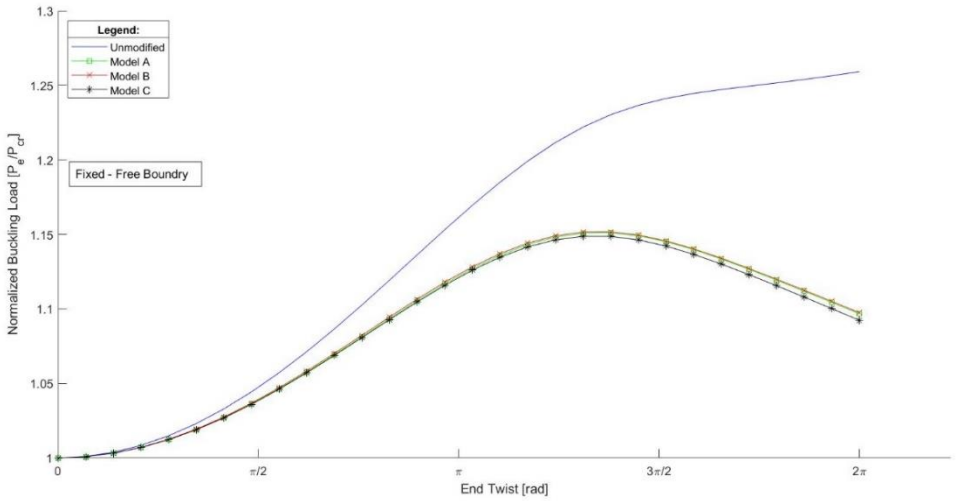

Fig. 8. Buckling load based on modified and unmodified theory for fixed-free support of the bar.

It seems that the results presented in Figs 5-8 are self-explanatory and clearly saying that the modifications proposed in this work have profound influence on mechanics of the pre-twisted bars. And those modifications have been introduced using simple physical arguments and a few fundamental principles of mechanics. No basic assumptions typically taught to define the mechanical behavior of simplified models, such as the Euler-Bernoulli assumptions about the cross-section's rigidity and orthogonality to the centroidal axis of the bar, are altered.

An encouraging aspect of the numerical illustrations presented here is that the results based on equations of structural mechanics of bars and those based on the three-dimensional potential energy are very close. This can be taken as confirmation of both. Of course, that was to a degree expected, because stationary condition of the potential energy is just a different way of expressing equilibrium, and all approximations in both approaches were otherwise identical. However, the nonlinearity in both of them was introduced in a somewhat different way: in potential energy formalism it was included in the entire volume of the bar while structural mechanics equations permitted that

only along the centroidal line of it. Thus, some differences between the two approaches were also expected. Less expected was the small influence of the torsional moment *T* exposed by the comparisons of Models A and B - its complete elimination from analysis only minimally changes the computed values, although those changes gradually increase with the amount of twist.

Even though the non-symmetric formulations based on structural mechanics equations was used in Model B (eq. (38)) all eigenvalues turned out to be real. This is another sign of how small effect the torsional moment *T* has in the range of twist considered in the calculations. But it is also a sign that relegating the non-symmetric contribution to the bar boundaries, as done in eq. (38), also helps since calculations based on eq. (37) did yield a few higher-order eigenvalues complex, with extremely small imaginary parts. The results of those calculations are not shown, since they were indistinguishable from the calculations based on eq. (38).

What the curves in Figs 5-8 illustrate is a competition between the strengthening effects related to the increasing contribution of the stronger axis moment of inertia and the weakening effects related to the weighting functions in the moments and products of inertia. For small pre-twist angles the strengthening effect dominates, but with increasing twist that effect stabilizes (cf. Tabarrok et al., 1990) while the weakening effect is continuously growing. To illustrate what happens when cross sections of other dimensions are analyzed and when larger range of the relative twist is considered the results for a bar with pin-pin boundary conditions are presented in Fig. 9. To better appreciate the effects of the proposed modifications the unmodified results for the same set of cross sections, the same support conditions and the same range of twist are also presented in Fig. 10. For other support conditions the behavior is qualitatively similar, and the difference is equally dramatic, but they are not telling any new story and, thus, not presented here.

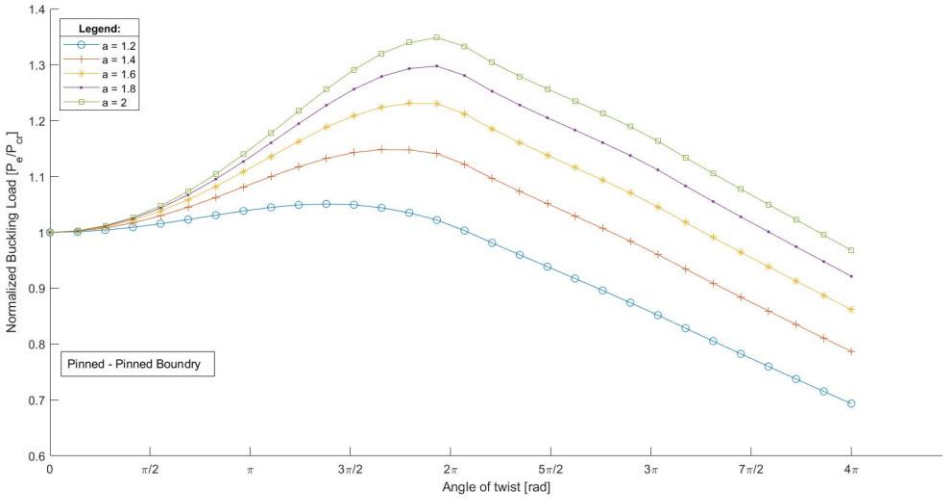

Fig. 9. Buckling load based on modified theory

for pinned-pinned support, variable *a* and *b=1*.

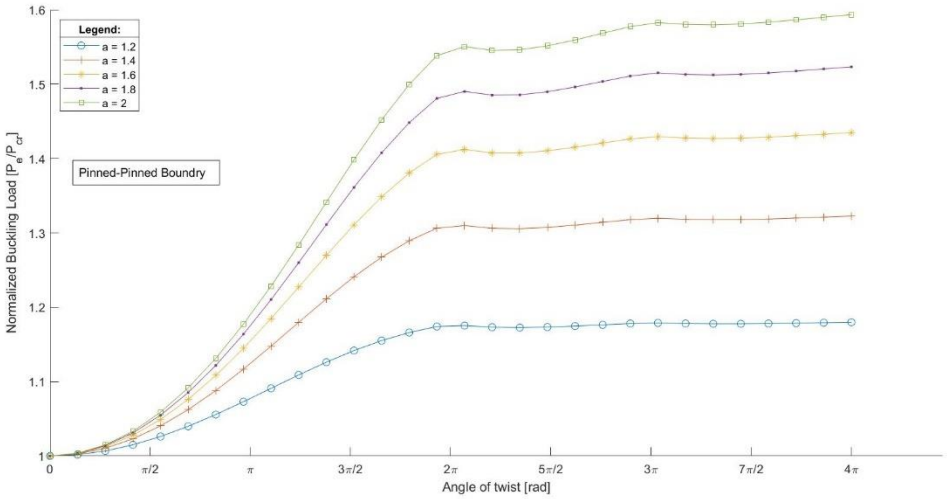

Fig. 10. Buckling load based on unmodified theory

for pinned-pinned support, variable *a* and *b=1*.

8. Concluding Comments.

The overall direction of research reported in this work was based on anticipation that in a pre-twisted bar axial force should produce a torque. It was expected that the torque would constitute an additional prestressing force, and that would change the critical buckling load.

Those expectations were in principle confirmed: generation of torque *T* could be logically justified and its contribution to the buckled bar's equilibrium quantified. But, as shown by the numerical examples, those contributions are practically negligible. It is likely that such a small effect of torque *T* has to do with a small rate of twist in bars, because in wire ropes, where that rate is much higher, torque *T* plays a significant role (Raoof and Kraincanic, 1995). And in the pre-twisted bars its effects also seem to gradually increase with the increasing rate of twist.

The formal process directed to identify *T* and quantify its influence on stability, led to weighted moments and product of inertia that, unexpectedly, had much more profound effect on the results than tension-generated torque. That effect appears to be significant even for relatively small amount of pre-twist, and these results will be of significant interest to a wider professional community. What has been found here was unexpected because it was (and still is) difficult to accept that such a strong effect has not been uncovered in the past in spite of a rather long list of publications on the subject (of which only representative selection is cited here).

Torque *T* has been associated with some essential formal difficulties of a different kind before it was uncovered how small effects it had. As a resultant force, *T* could be introduced only into the structural mechanics equations. However, the weak formulation of those equations, needed for the finite element numerical solution, was not symmetric and, as such, likely to furnish complex eigenvalues. To hopefully mitigate the problem two alternative approaches were followed. One of them was still based on structural mechanics equations but moved the non-symmetric terms to the bar's boundaries (Model B). The other one abandoned the structural mechanics approach

altogether and used three-dimensional continuum mechanics as a starting point (model C). Both of those models are presented in this work for illustration. In the latter approach the torque is introduced only indirectly, by the fact that the strain energy is assigned to the total strains (or stresses) aligned with the helixes, which includes the components normal and tangent to cross sections.

In retrospect, the convoluted path followed here to understand the problem had to do with attaching undue expectations to torque *T*. At the end it is clear that the effects of torque on stability can be safely neglected in all formulations presented here. However, without such a pursuit to quantify the effects of *T* the reduction in bending stiffness would still remain uncovered. May be that is why it was missed till now. The specific reduction used in this work is obviously a direct result of the assumed stress distribution. However, the logic presented in its support clearly demonstrates that some reduction should definitely be present even if a different stress distribution is assumed, but one that guarantees the stress-free boundary conditions on the side faces of the bar.

When torque *T* is neglected and it can be, as shown here, and the description of the problem uses displacements parallel to principal axis of the cross sections, the resulting differential equations of the modified theory will be like those in (Tabarrok et al., 1990), for example, but with weighted moments and product of inertia, of course. So, the solution approach pursued there can also be used to solve the problem described by the modified theory presented here.

Even though the significance of the proposed modifications has been documented here by the numerical results related to stability of bars, the proposed modifications should be of comparable importance in analysis of bending of pre-twisted structural members. After all, bending is a part of buckling discussed in this work and it is only the modification of the bending part of it that affects the stability results so much. That effect should be equally significant in analysis of biological and engineering structures,

considering that theory of pre-twisted bars is applied to both, as discussed in the Introduction.

The principal arguments used in this work were presented using the rectangular cross section as an example. The rectangular cross section has also been used in the numerical examples. That is arguably sufficient as a proof of concept, and rectangular cross sections are probably the most common in practical applications. But how well the proposed concepts would work for other cross sections needs to be examined independently. It is anticipated, however, that in comparison with the solutions based on the theory used in the past, application of theory proposed here to other shapes of the cross section would lead to differences of magnitude similar to that shown here for the rectangular shapes.

9. Bibliography.

Abid, S., Taktak, M., Dammak, F., et al., 2008. An accurate two-node finite element for the pre-twisted beam modelling. J. Mech. Eng. 59, 135–150.

Anliker, M., Troesch, B. A., 1963. Lateral vibration of pretwisted rods with various boundary conditions. ZAMP 14, 218-236.

Banchoff, T.F., Lovett, S., 2022. Differential Geometry of Curves and Surfaces, 3rd edition. CRC Press.

Bathe Klaus-Jürgen,1996, Finite element procedures. 274,314-330,537-550,702

Carnegie, W., 1964. Vibrations of pre-twisted cantilever blading allowing for rotary inertia and shear deflection. J. Mech. Eng. Sci. 6, 105–109.

Celep, Z., 1984. Finite element stability analysis of pre twisted Beck's column. Ingenieur-Archiv 54,337-344.

Frisch-Fay, R., 1973. Buckling of pre-twisted bars. Int. J. Mech. Sci. 15, 171-181.

Gangwar, T., Heuschele, DJ., Annor, G., Fok, A., Smith, KP., Schillinger, D., 2021. Multiscale characterization and micromechanical modeling of crop stem materials. Biomechanics and modeling in mechanobiology **20** (1), 69-91.

Gilmanov, A., Stolarski, H., Sotiropoulos, F., 2018. Flow–structure interaction simulations of the aortic heart valve at physiologic conditions: The role of tissue constitutive model. Journal of biomechanical engineering 140 (4).

Hamilton, W.C., Stolarska, M.A., Ismat, A., 2022. Simulation and in vivo experimentation predict AdamTS-A location of function during caudal visceral mesoderm migration in Drosophila. Dev Dyn. **251**(7):1123-1137.

Ji, X.Y., Zhao, M.Q., Wei, F., et al., 2012. Spontaneous formation of double helical structure due to interfacial adhesion. Appl. Phys. Lett. 100, 263104.

Raoof M., Kraincanic, I., 1995. Simple derivation of the stiffness matrix for axial/torsional coupling of spiral strands. Computers & Structures **55** (4), 589-600.

Le, B.L., Christenson, A., Calderer, T., Stolarski, H., Sotiropoulos, F., 2020. A thin-walled composite beam model for light-weighted structures interacting with fluids. Journal of Fluids and Structures, 95, 102968??

Lotz, B., Gonthier-Vassal, A., Brack, A., et al., 1982. Twisted single crystals of Bombyx mori silk fibroin and related model polypeptides with β structure: A correlation with the twist of the β sheets in globular proteins. J. Mol. Biol. 156, 345–357.

Malvern L.E. 1969. Introduction to the Mechanics of a Continuous Medium. Prentice-Hall.

Megahed, M., 2015. Buckling of Pretwisred Steel Columns. M.Sc. Thesis, American University of Sharjah College of Engineering. United Arab Emirates.

Reddy, J.N., 2018, Introduction to the Finite Element Method 4E. 80,155-328, 422-427

Schulgasser, K., Witztum, A., 2004a. Spiralling upward. J. Theor. Biol. 230, 275–280.

Schulgasser, K., Witztum, A., 2004b. The hierarchy of chirality. J. Theor. Biol. 230, 281–288.

Sinha, S.K., 2007. Combined Torsional-Bending-Axial Dynamics of a Twisted Rotating Cantilever Timoshenko Beam With Contact-Impact Loads at the Free End. Journal of Applied Mechanics, 74, 505-522.

Steinman, D., 1989. Exact solutions for the buckling analysis of pretwisted columns under various boundary conditions. M.Sc. Thesis, Department of Mechanical Engineering, University of Toronto.

Tabarrok, B., Yuexi, X., Steinman, D., et al., 1990. On buckling of pretwisted columns. Int. J. Solids Struct. 26, 59–72.

Wang, J.S., Wang, G., Feng, X.Q., et al., 2013. Hierarchical chirality transfer in the growth of Towel Gourd tendrils. Sci. Rep. 3, 3102.

Wang, X., Sturegård, E., Rupar, R., et al., 1997. Infection of BALB/c A mice by spiral and coccoid forms of Helicobacter pylori. J. Med. Microbiol. 46, 657–663.

Wempner, G., 1973. Machanics of Solids with Application to Thin Solids. McGraw-Hill.

Zhu, T.L., 2011. The vibrations of pre-twisted rotating Timoshenko beams by the Rayleigh-Ritz method. Comput. Mech. 47, 395– 408.

Zhao, Z-L., Zhao, H-P., Chang, Z, Feng, X-Q., 2014. Analysis of bending and buckling of pre-twisted beams: A bioinspired study. Acta Mechanica Sinica **30**(4):507–515.

Ziegler, H., 1951. Stabilitätsprobleme bei geraden Stäben und Wellen. ZAMP **2**, 265–289.